Inorg. Chem. **2003**, *42*, 6503–6518

Pressure-Induced Enhancements of Luminescence Intensities and Lifetimes Correlated with Emitting-State Distortions for Thiocyanate and Selenocyanate Complexes of Platinum(II) and Palladium(II)

John K. Grey,[†] Ian S. Butler,[†] and Christian Reber*[,‡]

Department of Chemistry, McGill University, Montreal, Quebec, H3A 2K6 Canada, and Département de chimie, Université de Montréal, Montréal, Québec, H3C 3J7 Canada

Received March 7, 2003

The luminescence properties of thiocyanate and selenocyanate platinum(II) and palladium(II) complexes show strong variations with temperature and pressure. The d–d luminescence band maxima for $[Pt(SCN)_4](PPh_4)_2$ (**1**), $[Pt(SCN)_4](n\text{-}Bu_4N)_2$ (**2**), and $[Pt(SeCN)_4](n\text{-}Bu_4N)_2$ (**4**) complexes are centered at ca. 14500 cm^{-1} whereas those of the $[Pd(SCN)_4](n\text{-}Bu_4N)_2$ (**3**) and $[Pd(SeCN)_4](n\text{-}Bu_4N)_2$ (**5**) complexes are approximately 2000 cm^{-1} lower in energy. Low-temperature luminescence spectra from single-crystal samples have broad bands with highly resolved vibronic structure indicating large displacements of the emitting-state potential energy minimum along several metal–ligand normal coordinates. The largest displacements involve the totally symmetric (a_{1g}) stretching modes with frequencies of 295 cm^{-1} (**1**), 303 cm^{-1} (**2**), 274 cm^{-1} (**3**), 195 cm^{-1} (**4**), and 185 cm^{-1} (**5**). The lower frequencies of these dominant progression-forming modes for the selenocyanate complexes lead to luminescence bands that are narrower by ca. 500 cm^{-1} (fwhm) than those observed from the thiocyanate complexes. Under external pressures, the room-temperature luminescence intensities and lifetimes show considerable enhancement at pressures up to 40 kbar. This effect is largest for the palladium(II) complexes with lifetimes increasing from approximately 350 ns at ambient pressure up to 62 μs at 30 kbar, an increase by more than 2 orders of magnitude. The platinum(II) complexes exhibit a significant, but noticeably lesser increase of luminescence lifetimes and intensities with increasing pressure. The temperature- and pressure-dependent luminescence decay behavior is rationalized using the emitting-state molecular geometry determined from the resolved low-temperature luminescence spectra combined with the strong-coupling limit of radiationless decay theory.

Introduction

Square-planar, d^8, platinum(II) and palladium(II) complexes show a wide range of luminescence properties that depend strongly on the structural and electronic characteristics of the ligands. It is well-known that the nature of the emitting-state and luminescence energies of these compounds can be tuned by substitution of ligands, by modification of ligand substituent groups, and by changes in the surrounding medium of the luminescent molecule, i.e., solvent, counterions, and neighboring complexes.[1−7] In addition to this chemical tuning, variation of temperature and pressure provides insight into the extent of tunability of electronic and vibronic transitions for a variety of transition metal complexes.[8−17] These variables can be used to characterize

* Author to whom correspondence should be addressed. E-mail: reber@chimie.umontreal.ca.
[†] McGill University.
[‡] Université de Montréal.

(1) (a) Cummings, S. D.; Eisenberg, R. *J. Am. Chem. Soc.* **1996**, *118*, 1949. (b) Zuleta, J. A.; Bevilacqua, J. M.; Eisenberg, R. *Coord. Chem. Rev.* **1991**, *111*, 237.
(2) Gliemann, G.; Yersin, H. *Struct. Bonding* **1985**, *62*, 87.
(3) Martin, D. S. *Inorg. Chim. Acta Rev.* **1971**, *5*, 107.
(4) (a) Connick, W. B.; Henling, L. M.; Marsh, E. M.; Gray, H. B. *Inorg. Chem.* **1996**, *35*, 6261. (b) Yang, F.; Fanwick, P. E.; Kubiak, C. P. *Inorg. Chem.* **2002**, *41*, 4805.
(5) Barigelletti, F.; Sandrini, D.; Maestri, M.; Balzani, V.; von Zelewsky, A.; Chassot, L.; Jolliet, P.; Maeder, U. *Inorg. Chem.* **1988**, *27*, 3644.
(6) Aldridge, T. K.; Stacy, E. M.; McMillin, D. R. *Inorg. Chem.* **1994**, *33*, 722.
(7) Yersin, H.; Trümbach, D.; Wiedenhofer, H. *Inorg. Chem.* **1999**, *38*, 1411.
(8) Ferraro, J. R. *J. Chem. Phys.* **1970**, *53*, 117.
(9) Bray, K. L.; Drickamer, H. G.; Schmitt, E. A.; Hendrickson, D. N. *J. Am. Chem. Soc.* **1989**, *111*, 2849.
(10) Bray, K. L., Drickamer, H. G. *J. Phys. Chem.* **1990**, *94*, 2154.
(11) Bray, K. L.; Drickamer, H. G. *J. Phys. Chem.* **1991**, *95*, 559.
(12) Gutierrez, R. E.; Rodriguez, F.; Moreno, M.; Alcala, R. *Radiat. Eff. Defects Solids* **2001**, *154*, 287.

10.1021/ic0342503 CCC: $25.00
Published on Web 09/06/2003

the effects of small changes in molecular geometry on kinetic competition between radiative and nonradiative excited-state relaxation,[18−21] coupling between potential energy surfaces,[22,23] or changes in the ground-state electronic structure, such as spin-crossover transitions.[24,25] We present a new pressure effect leading to large increases of luminescence intensities and lifetimes. It is specific to square-planar complexes with a Jahn−Teller active emitting state.

The title complexes have some unique traits relevant for the spectroscopic effects presented and discussed in the following. The ambidentate ligands, denoted as XCN^- (X: S, Se), may coordinate to the metal via the sulfur or selenium atom or via the nitrogen atom depending on the hardness or softness of the metal center.[26−30] All complexes studied here are coordinated through the X atom and have exact D_{4h} point group symmetry for the MX_4 fragment. Crystal structures for the title complexes show M−X−C angles of approximately 109° and 105−107° for the thiocyanate and selenocyanate complexes, respectively, and it was determined that the anionic complexes occupy only one site throughout the monoclinic lattice.[31] A recent normal coordinate analysis for the title complexes[31] has assigned the vibrational modes in idealized D_{4h} point group symmetry, and we use these labels for the ground-state metal−ligand vibrational modes (a_{1g}, b_{1g}, and b_{2g}) to characterize the resolved structure in the low-temperature luminescence spectra. The typical ranges of these frequencies are 274−303 cm^{-1} (a_{1g} totally symmetric stretching), 260−290 cm^{-1} (b_{1g} non-totally symmetric stretching), and 140−150 cm^{-1} (b_{2g} non-totally symmetric bending) for the SCN^- complexes, and 180−195 cm^{-1} (a_{1g}), 170−187 cm^{-1} (b_{1g}), and 100−110 cm^{-1} (b_{2g}) for the $SeCN^-$ complexes. We then determine if this difference in metal−ligand vibrational frequencies between the thiocyanate and selenocyanate complexes affects the variation in luminescence properties brought on by increasing pressure.

The electronic configuration of all title complexes is $a_{1g}(d_z^2)^2b_{2g}(d_{xy})^2e_g(d_{xz,yz})^2b_{1g}(d_{x^2-y^2})^0$, leading to a nondegenerate $^1A_{1g}$ ground state, and all one-electron excitations populate the b_{1g} σ^* orbital and are therefore interconfigurational. The lowest energy excited state is degenerate (^3E_g), originating from the promotion of an electron from the e_g orbitals to the b_{1g} orbital.[32−35] This state is split into five components by spin−orbit coupling. Low-temperature absorption spectra of the potassium salts of platinum(II) and palladium(II) thiocyanate complexes show broad and unresolved bands for the transition to this excited state, suggesting a superposition of the energetically close spin−orbit states.[32,36,37] Polarized absorption spectra of these complexes also show weak dichroisms for this transition.[36] Similar absorption features are observed for the title complexes, and the luminescence transition studied occurs from the lowest energy spin−orbit component of this state.[38]

The luminescence bands of the title complexes are broad, indicating large displacements of the emitting-state potential energy minimum along Franck−Condon active metal−ligand vibrational modes. These large structural distortions lead to weak luminescence at higher temperatures due to efficient nonradiative deactivation of the emitting state. At ambient temperature and pressure, the luminescence intensities of the title complexes and related compounds are very low and almost unobservable.[32,37] As temperature is lowered, the efficiency of nonradiative decay pathways is reduced and all title complexes show rapidly increasing luminescence intensities and lifetimes. Below 50 K, all luminescence spectra exhibit resolved vibronic structure with progressions in multiple vibrational modes, including the b_{2g} and b_{1g} metal−ligand non-totally symmetric bending and stretching modes. The vibronic structure is richer than for square-planar palladium(II) and platinum(II) halide complexes, where distortions only occur along a single non-totally symmetric mode.[37,39] The well-resolved vibronic structure of the title complexes allows for a detailed analysis of emitting-state distortions that may be used to rationalize the large pressure-induced effects on luminescence properties.

We have reported in a recent communication that the luminescence intensities and lifetimes of the $[Pd(SCN)_4](n\text{-}Bu_4N)_2$ complex show large increases under external pressures at room temperature.[40] The degree to which this effect depends on the nature of the metal center and ligands is now determined. All pressure-dependent luminescence intensities and lifetimes measured at room temperature show large increases in intensities and lifetimes, by almost 3 orders of magnitude, with the application of relatively modest pressures

(13) Wenger, O. S.; Valiente, R.; Güdel, H. U. *J. Chem. Phys.* **2001**, *115*, 3819.
(14) Wenger, O. S.; Güdel, H. U. *Chem. Phys. Lett.* **2002**, *354*, 75.
(15) Willett, R. D.; Haugen, J. A.; Lebsack, J.; Morrey, J. *Inorg. Chem.* **1974**, *13*, 2510.
(16) Dreger, Z. A.; Lang, J. M.; Drickamer, H. G. *J. Phys. Chem.* **1996**, *100*, 4646.
(17) Bloomquist, D. R.; Willett, R. D. *Coord. Chem. Rev.* **1982**, *47*, 125.
(18) Fetterolf, M. L.; Offen, J. *J. Phys. Chem.* **1985**, *89*, 3320.
(19) Fetterolf, M. L.; Offen, J. *J. Phys. Chem.* **1986**, *90*, 1828.
(20) Fetterolf, M. L.; Offen, J. *Inorg. Chem.* **1987**, *26*, 1070.
(21) Yersin, H.; Gallhuber, E. *Inorg. Chem.* **1984**, *23*, 3745.
(22) Grey, J. K.; Triest, M.; Butler, I. S.; Reber, C. *J. Phys. Chem. A* **2001**, *105*, 6269.
(23) Grey, J. K.; Butler, I. S.; Reber, C. *J. Am. Chem. Soc.* **2002**, *124*, 11699.
(24) Gütlich, P.; Hauser, A.; Spiering, H. *Angew. Chem., Intl. Ed. Engl.* **1994**, *33*, 2024.
(25) Grey, J. K.; Marguerit, M.; Butler, I. S.; Reber, C. *Chem. Phys. Lett.* **2002**, *366*, 361.
(26) Turco, A.; Pecile, C. *Nature* **1961**, *191*, 66.
(27) Pearson, R. G. *J. Am. Chem. Soc.* **1963**, *85*, 3533.
(28) Pearson, R. G. *Science* **1966**, *151*, 172.
(29) (a) Bertini, I.; Sabatini, A. *Inorg. Chem.* **1966**, *5*, 1025−1028. (b) Meek, D. W.; Nicpon, P. E.; Imhof-Meek, V. *J. Am. Chem. Soc.* **1970**, *92*, 5351. (c) Coyer, M. J.; Herber, R. H.; Chen, J.; Croft, M.; Szu, S. P. *Inorg. Chem.* **1994**, *33*, 716.
(30) Burmeister, J. L.; Basolo, F. *Inorg. Chem.* **1964**, *3*, 1587.
(31) Rohde, J.-U.; von Malottki, B.; Preetz, W. *Z. Anorg. Allg. Chem.* **2000**, *626*, 905.
(32) Pelletier, Y.; Reber, C. *Inorg. Chem.* **2000**, *39*, 4535.
(33) Basch, H.; Gray, H. B. *Inorg. Chem.* **1967**, *6*, 365.
(34) Vanquickenborne, L. G.; Ceulemans, A. *Inorg. Chem.* **1981**, *20*, 796.
(35) Harvey, P. D.; Reber, C. *Can. J. Chem.* **1999**, *77*, 16.
(36) Tuszynski, W.; Gliemann, G. *Z. Naturforsch.* **1979**, *34a*, 211.
(37) Pelletier, Y.; Reber, C. *Inorg. Chem.* **1997**, *36*, 721.
(38) The lowest energy spin−orbit state is A_{1g} (^3E_g) determined from ligand-field calculations included in the Supporting Information.
(39) Preston, D. M.; Güntner, W.; Lechner, A.; Gliemann, G.; Zink, J. I. *J. Am. Chem. Soc.* **1988**, *110*, 5628.
(40) Grey, J. K.; Butler, I. S.; Reber, C. *J. Am. Chem. Soc.* **2002**, *124*, 9384.

up to 30 kbar. The palladium(II) complexes show the largest pressure-induced increases. The effects for the platinum(II) complexes are significant, but weaker than the palladium(II) compounds. Similar pressure-dependent lifetime measurements on doped chromium(III) ions in various oxide, chloride, and fluoride lattices also show large increases, typically by 2 orders of magnitude, due to a change in emitting state from a spin-allowed $^4T_{2g}$ to a spin-forbidden ^2E_g, but no intensity increases have been reported.[41] Other studies have been carried out on molecular transition metal complexes that maintain the same emitting state with increasing pressure, such as polypyridyl complexes of ruthenium(II) and osmium(II).[18,19] These systems show only small variations of pressure-dependent luminescence lifetimes at constant temperature by less than a factor of 2 within similar pressure ranges as studied here.

Theoretical models are employed for calculating luminescence spectra as well as the trends of the temperature- and pressure-dependent luminescence decay behavior. The low-temperature luminescence spectra are analyzed using the time-dependent theory of spectroscopy,[42−45] which allows for the quantitative determination of the emitting-state distortions along all relevant normal modes and provides an intuitive means of understanding the detailed spectroscopic features. The experimental temperature-dependent luminescence decay rate constants were analyzed with an analytical expression for the nonradiative rate constant in the strong-coupling limit of radiationless decay theory derived by Englman and Jortner.[46] We use experimental information determined directly from the resolved low-temperature spectra, such as vibrational energies, the energy of the electronic origin transition, and emitting-state distortions, to calculate nonradiative rate constants for each complex. Only a single adjustable parameter in the pre-exponential factor remains to fit the experimental luminescence decay rate constant at all temperatures studied. We are then able to rationalize the different magnitudes of the pressure-induced increase in luminescence lifetimes for all title complexes with the parameters determined from the low-temperature luminescence spectra and temperature-dependent luminescence lifetimes.

Experimental Section

Single crystals of $[Pt(SCN)_4](PPh_4)_2$ (**1**), $[Pt(SCN)_4](n\text{-}Bu_4N)_2$ (**2**), $[Pd(SCN)_4](n\text{-}Bu_4N)_2$ (**3**), $[Pt(SeCN)_4](n\text{-}Bu_4N)_2$ (**4**), and $[Pd(SeCN)_4](n\text{-}Bu_4N)_2$ (**5**) were prepared following literature methods.[31,47−49] Starting materials were purchased from Sigma-Aldrich and used without further purification. Complexes **1**−**3** were also prepared by dissolving crystals of $K_2[PtCl_4]$ or $K_2[PdBr_4]$ in water and adding an aqueous solution of KSCN in excess followed by gentle refluxing for 2 h. After rotary evaporation of water, the potassium salts of the thiocyanate compounds were recrystallized three times from hot 1-butanol. The compounds were then dissolved in acetonitrile to which an excess of $(n\text{-}Bu_4N)Cl\cdot 2H_2O$ or $(PPh_4)Br$ in acetonitrile was added. All compounds were recrystallized several times by slow evaporation of acetonitrile and analyzed by Raman, luminescence, absorption, and excitation spectroscopy. Raman spectra of the title complexes were measured at 295 and 77 K, and bands in the metal−ligand stretching and bending region show strong and sharp peaks with frequencies in excellent agreement with literature values.[31] The mode of ligation for the thiocyanate and selenocyanate ligands was confirmed from Raman spectroscopy by monitoring the CN stretching frequencies, and all compounds show strong and sharp single peaks between 2100 and 2110 cm^{-1} (Table 1), indicative that ligands are *not* coordinated through the nitrogen atom of the XCN^- ligands and are oriented around the metal center in a nearly equivalent fashion.[31]

Temperature- and Pressure-Dependent Spectra. Luminescence spectroscopic measurements were carried out using two different instruments. Samples were cooled in a microcryostat system (Janis ST-500) by pumping off liquid helium. The 488 and 514.5 nm lines of argon ion lasers (∼2 mW) were focused onto the crystals using a Renishaw 3000 imaging microscope system. The luminescence was collected and detected with a Peltier-cooled CCD camera. The other system used to record the luminescence spectra was a single-channel scanning spectrometer.[50] A continuous flow helium cryostat (Oxford CF 1204) was used to cool samples down to 5 K. Excitation sources were again the 488 and 514.5 nm lines of an argon ion laser (Spectra Physics Stabilite 2017) using the appropriate interference filters. Excitation was focused onto samples with a quartz lens and the luminescence collected at 90° by a spherical mirror, then dispersed through a 0.5 m monochromator (Spex 500M, 600 lines/mm grating) with a long-pass filter (Schott OG 550, RG 610) positioned at the entrance slit. The detection system was a cooled photomultiplier tube (Hamamatsu R928 or R406/ Products for Research TE 177RF cooler) connected to a photon counter (Stanford SR 400) or lock-in amplifier (Stanford SR 510) with the luminescence signal modulated with an optical chopper (Stanford SR 540), and the intensities were saved on a computer also used to control the wavelength. Luminescence spectra of complexes **2** and **3** in a glassy matrix (1:1 toluene−acetone) were measured at 5 K with concentrations on the order of 10^{-4} M. All luminescence spectra are corrected for instrument response[50] by calibration with a tungsten lamp (Oriel 63350). The corrected luminescence band shapes obtained with the two instruments are identical. Detector response characteristics vary strongly over the wavelength range of interest, and it is therefore important to compare results recorded with different instruments.

Pressure-dependent luminescence and Raman spectra were recorded using the microscope system described above. Pressure was applied to the solid samples by loading crystals into a gasketed diamond-anvil cell (DAC, High-Pressure Diamond Optics). The ruby (R_1) method was used to calibrate pressures,[51] and paraffin oil was the pressure-transmitting medium. All pressure effects reported here are reversible where, upon gradual release of external pressures, all quantities return to their normal values at ambient pressure.

Luminescence Lifetime Measurements. Temperature-dependent lifetimes were measured using the doubled output (532 nm) of a

(41) Bray, K. L. *Top. Curr. Chem.* **2001**, *213*, 1.
(42) Masson, S.; Triest, M.; Grey, J. K.; Reber, C. *Phys. Chem. Commun.* **2000**, 12.
(43) Heller, E. J. *J. Chem. Phys.* **1975**, *62*, 1544.
(44) Heller, E. J. *Acc. Chem. Res.* **1981**, *14*, 368.
(45) Zink, J. I.; Kim Shin, K.-S. In *Advances in Photochemistry*; Volman, D. H., Hammond, G. S., Neckers, D. C., Eds.; John Wiley: New York, 1991; Vol. 16, p 119.
(46) Englman, R.; Jortner, J. *Mol. Phys.* **1970**, *18*, 145.
(47) Burmeister, J. L.; Al-Janabi, M. Y. *Inorg. Chem.* **1965**, *4*, 962.
(48) Burmeister, J. L.; Williams, L. E. *Inorg. Chem.* **1966**, *5*, 1113.
(49) Forster, D.; Goodgame, M. L. *Inorg. Chem.* **1965**, *4*, 1712.
(50) Davis, M. J.; Reber, C. *Inorg. Chem.* **1995**, *34*, 4585.
(51) Piermarini, G. J.; Block, S.; Barnett, J. D.; Forman, R. A. *J. Appl. Phys.* **1975**, *46*, 2774.

Table 1. Spectroscopic Quantities from the Temperature-Dependent Luminescence Spectra in Figures 1−5

quantity	$[Pt(SCN)_4]$-$(PPh_4)_2$ (**1**)	$[Pt(SCN)_4]$-$(n\text{-}Bu_4N)_2$ (**2**)	$[Pd(SCN)_4]$-$(n\text{-}Bu_4N)_2$ (**3**)	$[Pt(SeCN)_4]$-$(n\text{-}Bu_4N)_2$ (**4**)	$[Pd(SeCN)_4]$-$(n\text{-}Bu_4N)_2$ (**5**)
E_{max} (cm^{-1})	14770	14440	12390	14180	12530
luminescence origin (cm^{-1})	17464	16806	14343	16330	14445
τ (μs)	(700 nm)	(700 nm)	(770 nm)	(740 nm)	(780 nm)
	285, 4 K	320, 5 K	947, 5 K	300, 5 K	279, 5 K
	173, 50 K	207, 50 K	282, 50 K	149, 75 K	180, 100 K
	81, 125 K	102, 100 K	153, 100 K	86, 125 K	75, 175 K
	41, 175 K	49, 150 K	19, 150 K	27, 200 K	12, 200 K
		0.3, 200 K			
main progression interval (cm^{-1})	295	303	274	195	185
absorption†/excitation‡ maximum (cm^{-1})	19660†	19460‡	16450‡	18700‡	16610‡
Stokes shift (cm^{-1})	4895	5020	4060	4520	4080
freq intervals in luminescence spectra (cm^{-1})	295 [303, a_{1g}][a,b]	300 [303, a_{1g}][a,b]	274 [274, a_{1g}][a,b]	195 [195, a_{1g}][a,b]	185 [179, a_{1g}][a,b]
[Raman freqs (cm^{-1})]	250 [b_{1g}][b]	150 [151, b_{2g}][a,b]	260 [260, b_{1g}][a,b]	160 [b_{1g}]	145 [b_{1g}]
	230	33	165	105 [102, b_{2g}][a,b]	110 [113, b_{2g}][a,b]
	220		135 [144, b_{2g}][a,b]	65	65
	175		113 [115][b]		
	145 [151, b_{2g}][a,b]		35		
	108 [b_{2g}][c]				
	70 [77, Π]				
	35				
	10				
$\hbar\omega_{CN}$ (cm^{-1})	2101, 2126 (strong, sharp)	2107 (strong, sharp)	2103 (sharp)	2108 (strong, sharp)	2105 (strong, sharp)

[a] Reference 31. [b] This work. [c] Observed in absorption spectrum at 5 K in Figure 2b.

Nd:YAG pulsed laser (Continuum Mini-Lite II, ~5 ns pulse width). Laser pulse energy was kept at approximately 1 mJ/pulse measured at the laser head. The luminescence was dispersed by the 0.5 m monochromator and detected using the same cooled photomultiplier tube described above. The signal was averaged and saved on a digital oscilloscope (Tektronix TDS 380) triggered by a photodiode (Thorlabs FDS 100). Luminescence lifetimes of all complexes were recorded at multiple wavelength intervals as a function of temperature, and these values vary by 2% or less across the luminescence bands. Decay traces were fitted with single- and double exponential functions using least-squares methods. Decay was assigned as single exponential when χ^2 was less than 0.003 for a single-exponential function, otherwise it was assigned as double exponential. Measurements were recorded between 5 and 275 K. At higher temperatures an accurate determination of lifetimes was difficult due to low signal-to-noise ratios of the luminescence intensities.

Pressure-dependent lifetime measurements were carried out using the same pulsed laser source. The excitation was focused into the DAC with a short focal length quartz lens, and the emitted light was detected with the cooled R928 photomultipler tube with either a red (Schott RG 610) or orange (Schott OG 590) long-pass filter. These measurements take advantage of the entire luminescence band, and good signal-to-noise ratios were obtained. Signals were acquired using the same detection equipment described above. To avoid heating effects on the sample and possible damage to the DAC, the laser was used in low-energy mode and the output power was approximately 500 μJ/pulse.

Excitation and Absorption Spectra. A Xe lamp filtered through water to remove IR radiation was used as the excitation source. The 0.5 m monochromator was used to scan the excitation wavelength, and the emitted light was dispersed through a 0.75 m monochromator (Spex 1800 II, 600 lines/mm grating).[50] A KV 418 UV cutoff filter was placed at the exit slit of the excitation monochromator, and either OG 550 (compounds **2** and **4**) or RG 645 filters (compounds **3** and **5**) were placed at the entrance slit of the luminescence monochromator. Excitation spectra were measured at the luminescence band maximum as well as other wavelengths across the luminescence bands. The detection systems were the same as that used in the luminescence measurements.

Absorption measurements were carried out with a Varian Cary 5E spectrometer. Samples **2**−**5** were dissolved in a 1:1 toluene/acetone solution, spectra were recorded at 300 and 77 K, and the concentrations were on the order of 10^{-4} M.[52]

Spectroscopic Results

The luminescence spectra from single crystals of the title complexes are broad, spanning up to 4500 cm^{-1}. Low-temperature data reveal well-resolved long vibronic progressions in multiple vibrational modes. The band maxima are ca. 14500 cm^{-1} for platinum(II) complexes (**1**, **2**, **4**) and ca. 12500 cm^{-1} for the palladium(II) complexes (**3**, **5**). These characteristics are comparable to those of luminescence spectra for other square-planar transition metal compounds reported in the literature.[32,36,37,39,53]

The 5 K luminescence and absorption spectra of **1** are shown in Figures 1 and 2 and serve as representative examples for typical luminescence and absorption spectral profiles of the title complexes at low temperature. The luminescence band has well-resolved vibronic structure with a main progression in the a_{1g} mode and an easily visible, but less intense progression matching the frequency of the b_{2g} non-totally symmetric bending mode. Additional structure is observable near the origin region, as shown in Figure 2a, and the frequencies of all relevant vibrational modes determined from the luminescence spectra are listed in Table

(52) Solution absorption spectra of all complexes have similar spectral profiles consisting of a weak, lowest energy band with a molar absorptivity on the order of 10 M^{-1} cm^{-1} with overlapping, more intense (ϵ > 100 M^{-1} cm^{-1}) transitions with maxima ca. 2500 cm^{-1} higher in energy. At approximately 340 nm (29000 cm^{-1}), there is an intense ($\epsilon \approx 103$ M^{-1} cm^{-1}) and sharp absorption band observed for all complexes studied.

(53) Güntner, W.; Gliemann, G.; Kunkely, H.; Reber, C.; Zink, J. I. *Inorg. Chem.* **1990**, *29*, 5238.

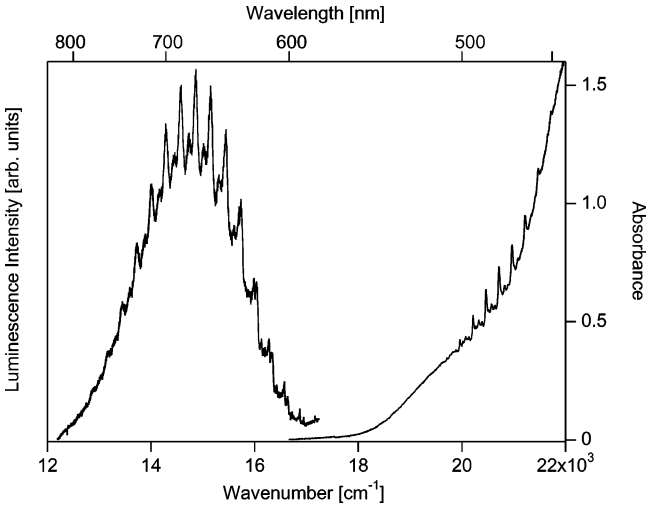

Figure 1. Single-crystal luminescence and unpolarized absorption spectra of $[Pt(SCN)_4](PPh_4)_2$ **1** at 5 K (unpolarized).

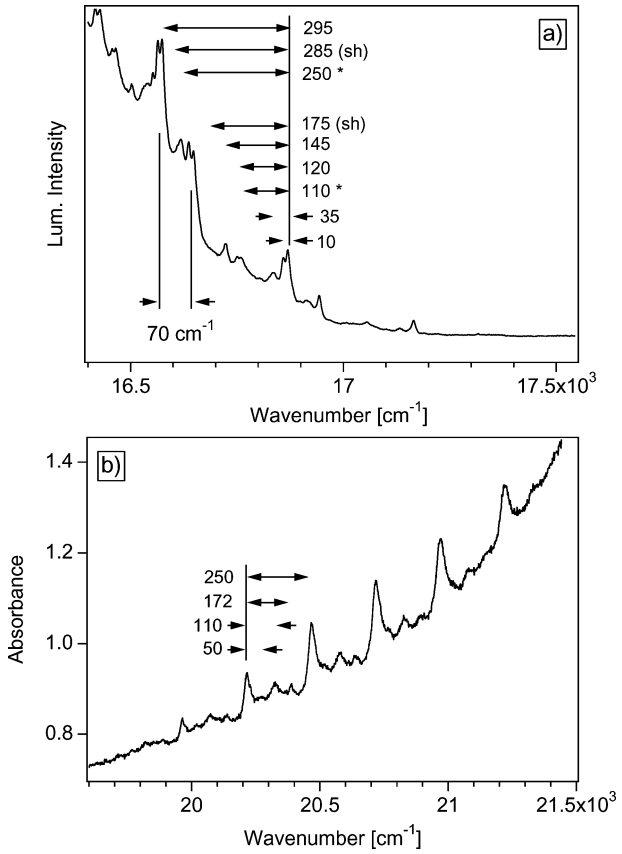

Figure 2. (a) High-resolution luminescence spectrum of $[Pt(SCN)_4](PPh_4)_2$ **1** at 5 K near the luminescence origin (E_0). The spectrum consists of two progressions that are separated by approximately 70 cm^{-1} and by additional small-frequency intervals of 35 and 10 cm^{-1}. Vibronic intervals in wavenumber (cm^{-1}) units are indicated on the spectrum; asterisks (*) correspond to vibrational quanta that also appear in the 5 K absorption spectrum, and "(sh)" stands for shoulder. (b) 5 K absorption spectrum of **1** showing details of the vibronic structure in the second, higher energy band in Figure 1.

1. The high-resolution spectrum in Figure 2a reveals that the dominant progressions are separated by small frequency intervals of 10, 35, and 70 cm^{-1}. These fine features are lost toward the band maximum where the intensities of the main vibronic bands are much higher. Up to 17 quanta of the a_{1g} stretching mode with an average frequency interval of 295 cm^{-1} on the blue side of the band are resolved in the 5 K luminescence spectrum with the band maximum at the 9th member of this progression. Starting from this member, the vibronic spacings decrease gradually by 11 cm^{-1} to 284 cm^{-1} at the 15th quantum. Polarized luminescence spectra of **1** were recorded at 20 K and show the same relative intensity distributions throughout the spectrum as in the unpolarized spectrum in Figure 1. The dichroic ratio of the total intensities is approximately 2 (shown in the Supporting Information). Luminescence intensities and lifetimes are strongly temperature dependent. Lifetimes increase by up to a factor of 300 between ambient temperature and 5 K, demonstrating efficient nonradiative relaxation processes at higher temperatures. The 5 K unpolarized absorption spectrum in Figure 1 has a weak and unresolved band for the lowest energy transition that corresponds to overlapping transitions to multiple spin−orbit components of the ^3E_g excited state.[34,35] However, there is another band starting at 19960 cm^{-1} that shows resolved vibronic structure in four discernible modes, as shown in detail in Figure 2b. The largest frequency interval in this resolved band is 250 cm^{-1}, which is most likely the frequency of the a_{1g} vibrational mode in this excited state. The Stokes shift between the luminescence band maximum and the center of the first absorption band in Figure 1 is approximately 4900 cm^{-1}, indicative of large structural changes along the metal−ligand vibrational modes. Estimated energy gaps between the onsets of the luminescence and absorption bands are found to be approximately 500 cm^{-1}, much smaller than those found in platinum(II) and palladium(II) complexes with simple halide ligands.[37,39] This energy gap probably arises from vibronic origins involving low-frequency odd-parity promoting modes.

Temperature-Dependent Luminescence Intensities and Lifetimes. Figures 3 and 4 show the temperature-dependent luminescence spectra and 5 K excitation spectra of the platinum(II) complexes (**2** and **4**) and palladium(II) complexes (**3** and **5**), respectively, and all relevant spectroscopic quantities referred to in the following are collected in Table 1. The luminescence spectra of these complexes exhibit well-resolved vibronic structure at temperatures below 50 K with the dominant progression-forming frequencies corresponding to the a_{1g} metal−ligand stretching mode in addition to prominent lower frequency progressions including the b_{2g} non-totally symmetric bending mode. Progressions in the b_{1g} non-totally symmetric stretching modes appear as weak shoulders on the blue side of a_{1g} vibronic bands. The low-temperature luminescence of **2**, Figure 3a, shows features similar to that of **1** with the luminescence band maximum shifted to lower energy by 330 cm^{-1}. This complex exhibits a more noticeable decrease in the main progression interval toward higher quanta of the a_{1g} mode than what is observed in the 5 K luminescence spectrum of **1** with the interval decreasing by as much as 30 cm^{-1} across the band. At the band maximum, close to the 10th member of the a_{1g} progression, the frequency interval is approximately 285 cm^{-1}, and by the 15th quantum the interval decreases to 270 cm^{-1}. The luminescence origin region is less resolved than for complex **1** in Figure 2a. However, a weak shoulder (∼33

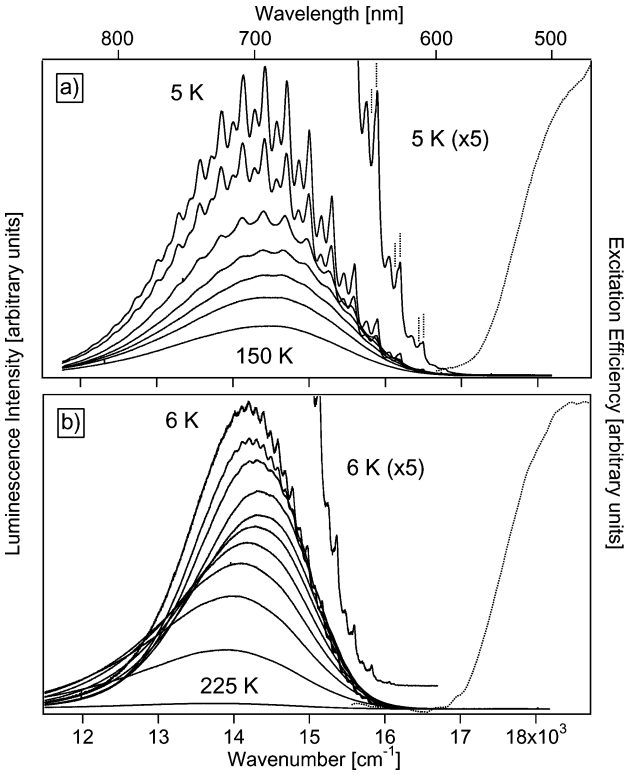

Figure 3. (a) Luminescence and excitation spectra of $[Pt(SCN)_4](n\text{-}Bu_4N)_2$ **2**. Temperature-dependent luminescence spectra are shown at 5, 25, 50, 75, 100, 125, and 150 K (top to bottom). The excitation spectrum at 5 K (dotted trace) shows the first absorption transition. The luminescence spectrum at 5 K is enlarged by a factor of 5 to show detailed features near the origin. Dotted vertical lines show the small experimental energy separation (35 cm^{-1}) resolved near the origin, but not across the entire band. (b) Luminescence and excitation spectra of $[Pt(SeCN)_4](n\text{-}Bu_4N)_2$ **4**. Temperature-dependent luminescence spectra at 6, 15, 30, 50, 75, 100, 125, 150, 175, 200, and 225 K are shown top to bottom. The excitation spectrum at 5 K (dotted trace) shows the first absorption transition. The luminescence spectrum at 6 K is enlarged by a factor of 5 and offset along the ordinate for clarity.

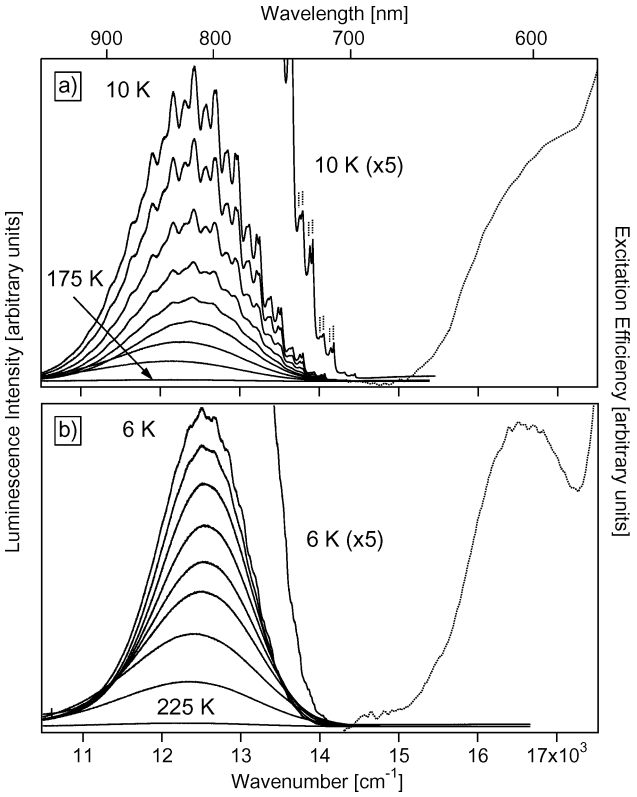

Figure 4. (a) Luminescence and excitation spectra of $[Pd(SCN)_4](n\text{-}Bu_4N)_2$ **3**. Temperature-dependent luminescence spectra are shown at 10, 20, 30, 45, 50, 60, 70, 100, 125, and 175 K (top to bottom). The luminescence spectrum at 5 K is enlarged by a factor of 5 to show the small repetitive spacings near the origin. Dotted vertical lines illustrate this separation of 35 cm^{-1} for this complex. (b) Luminescence and excitation spectra of $[Pd(SeCN)_4](n\text{-}Bu_4N)_2$ **5**. Temperature-dependent luminescence spectra at 6, 15, 30, 50, 75, 100, 125, 150, 175, and 225 K are shown top to bottom. The luminescence spectrum at 5 K is enlarged by a factor of 5 to show detailed features near the origin. The excitation spectra at 5 K (dotted traces) show the first absorption transition for both complexes **3** and **5**.

cm^{-1}) is observed on the red side of the a_{1g} interval near the luminescence origin and is subsequently lost toward the band maximum, as illustrated in Figure 4a with dotted vertical lines. To determine if the vibronic patterns persisted in a different medium, the luminescence spectra of **2** in a glassy matrix were measured at 5 and 77 K and gave broad and unresolved bands; however, the overall spectral profiles and band maxima were similar to the data obtained for single-crystal samples. When the $SeCN^-$ ligand replaces SCN^- on the metal centers, the luminescence spectrum becomes narrower as a result of the lower frequency Pt−SeCN modes that form vibronic progressions. The band maximum does not show an appreciable shift in energy, indicating very similar ligand fields for the two different ligands.[54] Figure 3b shows the luminescence of $[Pt(SeCN)_4](n\text{-}Bu_4N)_2$ (**4**) as a function of temperature. The 6 K luminescence spectrum exhibits well-resolved progressions in the 195 (a_{1g}) and 105 (b_{2g}) cm^{-1} modes in addition to less intense progressions in the 160 and 65 cm^{-1} modes that are not resolved toward the lower energy side of the band. The positions of the band maxima were also found to change as a function of temperature. At 225 K the band is centered at 13690 cm^{-1}; it then blue shifts gradually by approximately 600 cm^{-1} at 50 K. From 50 to 6 K, the band red shifts by 150 cm^{-1}. Excitation spectra of both **2** and **4** at 5 K show a weak and unresolved first absorption band, similar to that observed in the 5 K lowest energy absorption band of **1**, and excitation spectra monitored at different wavelengths across the luminescence bands all give the same results as shown in Figure 3. The Stokes shifts for complexes **2** and **4** are 5020 and 4520 cm^{-1}, respectively, and energy gaps between luminescence and excitation onsets are both comparable to the value determined for $[Pt(SCN)_4]^{2-}$ (**1**) in Figure 1.

Figure 4 shows the temperature-dependent luminescence spectra of $[Pd(SCN)_4](n\text{-}Bu_4N)_2$ (**3**) and $[Pd(SeCN)_4](n\text{-}Bu_4N)_2$ (**5**). The temperature-dependent luminescence spectra of the palladium(II) complexes behave in a manner similar to that of the platinum(II) complexes showing weak bands at high temperature. Vibronic structure in **3** is more resolved than spectra previously reported using different counterions.[32] Progressions in the b_{1g} non-totally symmetric stretching modes, in addition to the long progressions in the b_{2g} bending mode, are resolved as shoulders close to the maxima of the a_{1g} vibronic peaks. It is not possible to conclusively determine if there is an experimentally significant decrease in the a_{1g}

(54) Jørgensen, C. K. *Absorption Spectra and Chemical Bonding in Complexes*; Pergamon Press: London, 1962.

progression interval for complex **3**, as was observed in the low-temperature luminescence spectra of platinum(II) complexes **1** and **2**. The number of resolved peaks on the red side of the spectra is lower than for the platinum(II) analogues, preventing a detailed comparison to these compounds. Near the luminescence origin, complex **3** exhibits the most distinguishable repetitive patterns at temperatures below 20 K with well-resolved frequency differences of 35 cm^{-1} on each member of the dominant progressions. Luminescence spectra of this complex in a glassy matrix were measured at 5 K to observe this feature in a different environment; however, the results revealed broad and featureless bands. Vibronic structure in the selenocyanate analogue **5** is not as resolved as in the other complexes except near the origin region where small intervals of approximately 65 cm^{-1} are barely resolved. On the red side of the band, resolved structure is completely absent, similar to the platinum(II) complex **4**. In an attempt to achieve better resolution of vibronic structure by further separating the $[Pd(SeCN)_4]^{2-}$ luminophores in the crystal lattice, the tetrabutylammonium counterion was exchanged for the larger bis(triphenylphosphonium)phosphoranylidene ammonium $(PPN)^+$ cation, but the resulting 6 K luminescence spectrum showed no significant improvement. The excitation spectra of **3** and **5** show band shapes similar to those of the platinum(II) complexes **2** and **4**, and vibronic structure is virtually absent. Excitation maxima are 16450 cm^{-1} for **3** and 16610 cm^{-1} for **5**, both lower in energy by approximately 2000 cm^{-1} than the platinum(II) complexes. Stokes shifts for these two palladium(II) complexes are similar with values of 4060 cm^{-1} for **3** and 4080 cm^{-1} for **5**. The energy gaps between luminescence and excitation onsets are approximately 800 cm^{-1} for both palladium(II) complexes, somewhat larger than the literature value of 300 cm^{-1} for the $[Pd(SCN)_4]^{2-}$ luminophore in different crystalline environments.[32]

Figure 5 shows the temperature-dependent integrated luminescence intensities and lifetimes for complexes **2**−**5**. All luminescence lifetimes reported in Figure 5 and Table 1 were measured near the luminescence band maximum, and all show a similar increase, by up to a factor of 300, when temperature is decreased from 250 to 5 K. Complex **3** (Figure 5c) shows a slightly different behavior: its luminescence lifetimes increase drastically at temperatures lower than 50 K. The platinum(II) thiocyanates (**1**, **2**) exhibit double-exponential excited-state decay behavior with a fast component accounting for approximately 5% of the total intensity at 5 K, which is followed by a steady increase of the fast component to 50% at 150 K. This type of decay behavior is wavelength dependent and appears predominantly on the blue sides of the luminescence spectra of **1** and **2**. The fast component is assigned as a luminescent trap. Single- and double-exponential fit results for lifetimes measured from the high-energy onset (640 nm) to the band maximum (700 nm) are included in the Supporting Information.

Normalized integrated luminescence intensities for complexes **2**−**5** show steady decreases with increasing temperature, the exception again being complex **3** where, similar to the lifetimes, the intensity shows a large increase at

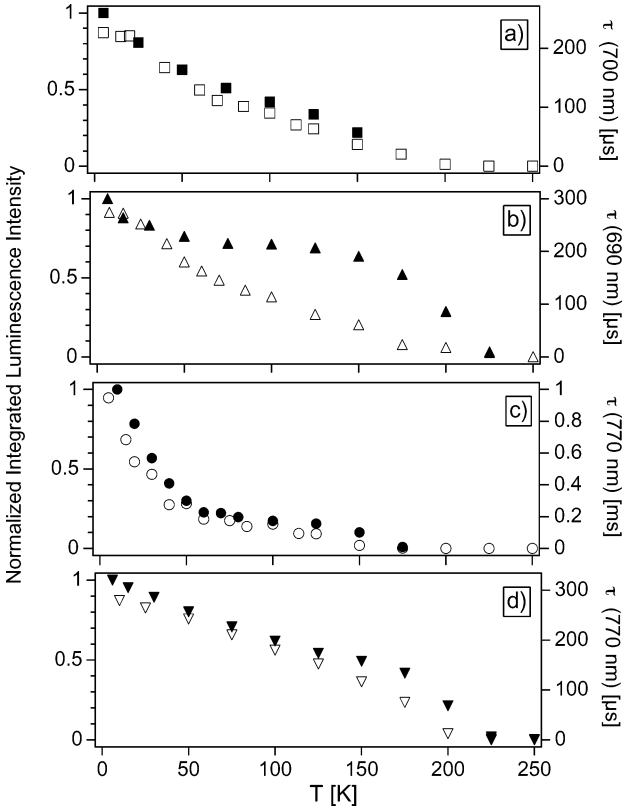

Figure 5. Normalized integrated luminescence intensities (solid symbols) and single-exponential luminescence lifetimes (open symbols) at wavelengths near the luminescence band maxima: (a) $[Pt(SCN)_4](n\text{-}Bu_4N)_2$ **2** (squares) at 700 nm; (b) $[Pt(SeCN)_4](n\text{-}Bu_4N)_2$ **4** (triangles) at 690 nm; (c) $[Pd(SCN)_4](n\text{-}Bu_4N)_2$ **3** (circles) at 770 nm; (d) $[Pd(SeCN)_4](n\text{-}Bu_4N)_2$ **5** (inverted triangles) at 770 nm.

temperatures lower than 50 K. The temperature-dependent integrated intensities all have weak shoulders in the temperature range 100−150 K. This feature is not seen in the lifetime data and is most evident in the intensity data of complex **4** (Figure 5b) where the integrated intensities change little between 75 and 150 K and then decrease rather suddenly at higher temperatures. Differences in the temperature-dependent luminescence intensities may be attributed to subtle changes in radiative and nonradiative relaxation rate constants and energy transfer rate constants. All compounds show a strong decrease of their luminescence intensity and lifetime at high temperatures, a key condition for the observation of the unusual pressure effects presented in the next section.

Pressure-Dependent Luminescence Intensities and Lifetimes. Figures 6−8 show pressure-dependent luminescence spectra and lifetimes of complexes **2**−**5** in a similar crystalline environment.[55] The pressure-induced changes in important spectroscopic quantities are summarized in Table 2. All complexes show large increases of luminescence intensities and lifetimes as a function of pressure, by almost 3 orders of magnitude between ambient pressure and 35 kbar at room temperature. This effect is accompanied by significant blue shifts of the luminescence band maxima by up to 29 cm^{-1}/kbar. Pressure-dependent Raman spectra are monitored

(55) Similar studies were performed on complex **1**. The overall pressure effect was similar to that of complex **2**.

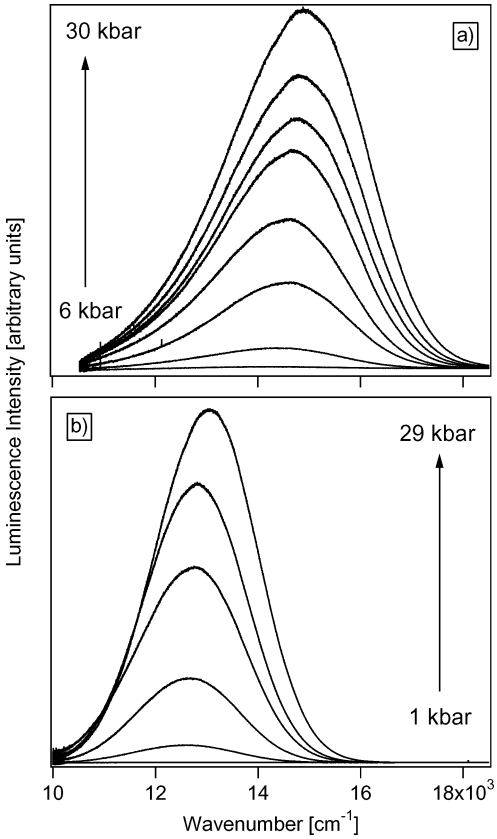

Figure 6. Representative pressure-dependent luminescence spectra for thiocyanate complexes: (a) $[Pt(SCN)_4](n\text{-}Bu_4N)_2$ **2** at 6, 10, 16, 17, 21, 24, 26, 28, and 30 kbar (bottom to top); (b) $[Pd(SCN)_4](n\text{-}Bu_4N)_2$ **3** at 1, 9, 12, 18, 27, and 29 kbar (bottom to top).

concomitantly to determine if changes in molecular structure accompany the unusual intensity and lifetime increase. Most spectra show similar smooth shifts of the metal−ligand vibrational bands to higher frequency as a function of pressure.

Figure 6 shows pressure-dependent luminescence spectra of **2** (Figure 6a) and **3** (Figure 6b) at pressures up to 30 kbar. The ambient pressure spectrum is very weak and appears as a flat trace at the bottom of each panel. As pressure is increased on the crystalline samples, the luminescence intensities show a fast, but continuous increase followed by a slow decrease at pressures over 30 kbar. The luminescence band maxima show a steady blue shift as a function of pressure with values of 24 cm^{-1}/kbar (**2**) and 29 cm^{-1}/kbar (**3**) (Table 2).[56] These shifts are opposite to those observed in the well-studied tetracyanoplatinate(II) complexes where there are strong metal−metal stacking interactions between the closely spaced $[Pt(CN)_4]^{2-}$ chromophores.[2,57] In the title systems, the closest distance for the metal centers to interact in a stacking fashion is approximately 13 Å,[31] larger by more than a factor of 3 than typical metal−metal distances of 3.1−3.7 Å in tetracyanoplatinate(II) complexes,[58] immediately

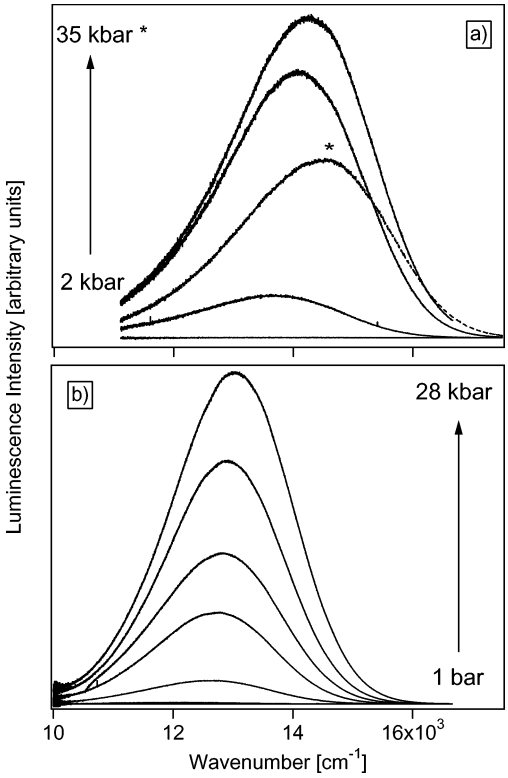

Figure 7. Representative pressure-dependent luminescence spectra for selenocyanate complexes. (a) $[Pt(SeCN)_4](n\text{-}Bu_4N)_2$ **4** at 2, 5, 16, 23, 25, and 35 kbar (bottom to top). The highest pressure spectrum (35 kbar) is indicated by an asterisk. (b) $[Pd(SeCN)_4](n\text{-}Bu_4N)_2$ **5** at 1 bar (ambient pressure), 2, 5, 11, 13, 20, and 28 kbar (bottom to top).

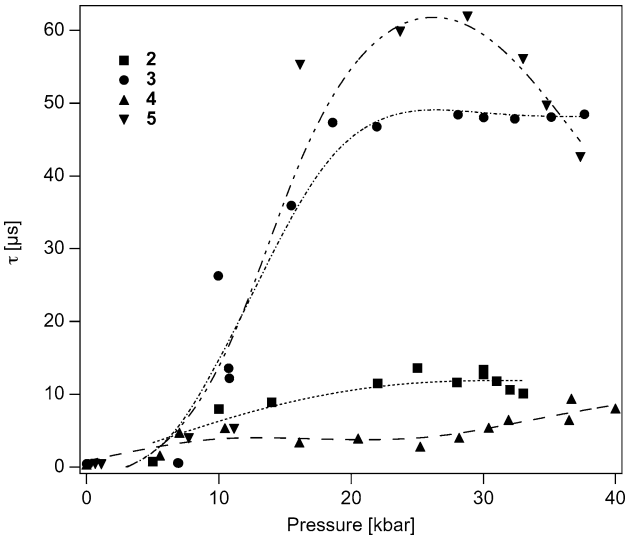

Figure 8. Pressure-dependent luminescence lifetimes: (a) $[Pt(SCN)_4](n\text{-}Bu_4N)_2$ **2** (squares); (b) $[Pd(SCN)_4](n\text{-}Bu_4N)_2$ **3** (circles); (c) $[Pt(SeCN)_4](n\text{-}Bu_4N)_2$ **4** (triangles); (d) $[Pd(SeCN)_4](n\text{-}Bu_4N)_2$ **5** (inverted triangles). The accompanying curves for each data set are included as a guide for the eye.

ruling out metal−metal interactions as a cause for the pressure effects reported here. The effect of pressure on the luminescence spectrum of $K_2[Pt(SCN)_4]$ has been previously studied at 100 K, and a blue shift of the band maximum of 10±3 cm^{-1}/kbar was found,[59] almost 3 times smaller than

(56) Blue shifts in the pressure-dependent luminescence band maximum were determined by fitting a Gaussian function to the spectrum using least-squares methods.
(57) Lechner, A.; Gliemann, G. *J. Am. Chem. Soc.* **1989**, *111*, 7469.
(58) Houlding, V. H.; Miskowski, V. M. *Coord. Chem. Rev.* **1991**, *111*, 145.
(59) Hidvegi, I.; Tuszynski, W.; Gliemann, G. *Chem. Phys. Lett.* **1981**, *77*, 517.

Table 2. Spectroscopic Quantities Obtained from the Pressure-Dependent Luminescence and Raman Spectra of the Title Complexes

quantity	$[Pt(SCN)_4](n\text{-}Bu_4N)_2$ (**2**)	$[Pd(SCN)_4](n\text{-}Bu_4N)_2$ (**3**)	$[Pt(SeCN)_4](n\text{-}Bu_4N)_2$ (**4**)	$[Pd(SeCN)_4](n\text{-}Bu_4N)_2$ (**5**)
ΔE_{max} (cm^{-1}/ kbar)	+24	+29	+12	+25
$\Delta\hbar\omega_{a_{1g}}$ (cm^{-1}/ kbar)	+0.60	+0.68	+0.46	+0.57
$\Delta\hbar\omega_{b_{2g}}$ (cm^{-1}/ kbar)	+0.88	+0.72	*a*	*a*
τ	750 ns (5 kbar)	541 ns (7 kbar)	2 μs (5 kbar)	4 μs (7 kbar)
	9 μs (14 kbar)	36 μs (15 kbar)	3 μs (16 kbar)	55 μs (16 kbar)
	13 μs (30 kbar)	48 μs (30 kbar)	6 μs (32 kbar)	62 μs (28 kbar)

[a] $\hbar\omega_{b_{2g}}$ peaks are too close to the Rayleigh cutoff filter used in the pressure-dependent Raman measurements.

the blue shift reported for **2**. This literature study also reports a very significant decrease of the luminescence intensity at 57 kbar. The linearly polarized luminescence spectra at 100 K exhibit a small dichroism, comparable to the polarized spectrum of **1** measured at 20 K, indicating that the nature of the luminescence transition is similar in $K_2[Pt(SCN)_4]$ and the $[Pt(SCN)_4]^{2-}$ complexes **1** and **2**. Figure 7 shows pressure-dependent luminescence spectra of the selenocyanate complexes, $[Pt(SeCN)_4](n\text{-}Bu_4N)_2$ (**4**) and $[Pd(SeCN)_4](n\text{-}Bu_4N)_2$ (**5**). Increases in luminescence intensities are similar to those in the thiocyanate analogues with the notable exception of complex **4**, whose enhancement of the signal is much smaller than that of all other complexes studied. The pressure-induced blue shifts for band maxima of the selenocyanates are 12 cm^{-1}/kbar (**4**) and 25 cm^{-1}/kbar (**5**). It is also interesting to note that the blue shift for complex **4** is lower by a factor of 2 than the observed blue shifts for the other complexes and more comparable to the literature value found for the $[Pt(SCN)_4]^{2-}$ complex with the smaller K^+ counterion.

Figure 8 shows the pressure-dependent luminescence lifetimes of complexes **2**−**5**. All experimental excited-state decay kinetics are single exponential, and all luminescence lifetimes increase with pressure. The largest enhancement occurs for the palladium(II) complexes where the lifetimes increase by almost 3 orders of magnitude from their ambient pressure values of approximately 350−400 ns up to 62 μs at 28 kbar. The platinum(II) complexes show much smaller increases in lifetimes, up to 15 μs at high pressures (ca. 30 kbar) from approximately 1 μs at ambient pressure. Complex **4** exhibits the smallest increase in lifetimes of all complexes studied, similar to the trends observed in luminescence intensities and blue shift of the band maxima as a function of pressure. At pressures greater than 30 kbar, all complexes tend to show slight decreases in both intensity and lifetime. Decreases in pressure-dependent luminescence intensity are quite common due to more efficient energy transfer processes between luminophores and to deep traps when the sample volume becomes smaller. Pressure increases inhomogeneity and possibly also the number of deep traps, further reducing the observed luminescence intensity. Evidence for this effect comes from pressure-dependent Raman spectra where measurements of **2** show noticeable changes in the intensities and number of bands in the metal−ligand stretching region (280−300 cm^{-1}), as shown in the Supporting Information. We rationalize the pressure effects using the detailed spectroscopic information obtained at low temperature.

Discussion

Vibronic Structure in Low-Temperature Luminescence Spectra. The well-resolved vibronic structure in the luminescence spectra presented in Figures 1−4 provides detailed insight into the structural changes which the title complexes undergo upon emission of a photon. We discuss the most important features, which are (a) long progressions in multiple modes, namely, the a_{1g} and b_{2g} stretching and bending modes, respectively; (b) vibronic origins arising from odd-parity vibrational modes; and (c) the small repetitive spacings near the luminescence origins. The low-temperature luminescence spectroscopy of **1** was used as a benchmark for illustrating the previous points because it shows the best resolution of the vibronic structure.

Long progressions in non-totally symmetric vibrational modes, as shown in Figures 1−4, are rare for square-planar complexes. The appearances of prominent frequency intervals in the b_{2g} bending mode and the b_{1g} stretching mode mean that the emitting-state geometry has a lower point group symmetry than the ground state.[60] The most plausible rationale for long progressions in a bending mode comes from previous low-temperature luminescence spectra of the $[Pd(SCN)_4]^{2-}$ luminophore in different crystalline environments than of those studied here, showing evidence of a progression in the b_{2g} mode.[32] DFT calculations qualitatively confirm the activity of the b_{2g} mode from the electron density on the highest occupied d-orbitals on the metal center, e_g (d_{xz}, d_{yz}), being tilted off-axis due to repulsive effects from the proximity of lone-pair electron density on the sulfur atoms of the thiocyanate ligands. By exciting an electron to the higher-lying b_{1g} ($d_{x^2-y^2}$) orbital, whose lobes are oriented on the bonding axes, this repulsive effect is altered, thereby favoring a scissor (b_{2g}) motion. Another possibility is that the b_{2g} interval appears due to progressions in the totally symmetric (a_{1g}) stretching mode built on vibronic (false) origins of promoting modes that differ by approximately the b_{2g} vibrational frequency. In D_{4h} point group symmetry the components of the electric dipole transform under the a_{2u} and e_u irreducible representations and a vibronically allowed transition will require 1 quantum of either a_{2u} or e_u vibrations. In the title complexes one of the two e_u modes has a frequency difference with the a_{2u} mode that could give rise to an interval between vibronic origins matching the b_{2g} frequency if both types of promoting modes are active.[61] For

(60) Sturge, M. D. *Solid State Phys* **1967**, *20*, 91.

(61) The experimental frequencies (ref 31) of the a_{2u} and the two e_u modes, $e_u(1)$:$e_u(2)$, for the title complexes are as follows (in cm^{-1}): 142 and 169,287 (**1**, **2**); 140 and 165,293 (**3**); not observed and 127,132: 221,236 (**4**); 96 and 121,128:242,259 (**5**), respectively.

the thiocyanate complexes, the appropriate e_u mode has a frequency difference between the a_{2u} mode within 5 cm^{-1} of the b_{2g} bending frequencies whereas this difference for the selenocyanate complexes is up to 30 cm^{-1} larger than the actual frequency interval observed in the resolved luminescence spectra in Figures 3b and 4b. The inclusion of the b_{2g} bending modes is therefore justified based on the experimental luminescence spectra in Figures 1−4.

It is important to point out that there is another e_u mode[62] approximately 25−35 cm^{-1} higher in frequency than the a_{2u} mode for all complexes, and the frequency difference between these two possible promoting vibrations may account for the repetitive spacings observed in the thiocyanate complexes in Figures 2a, 3a, and 4a. We first consider all other possibilities for the appearance of these small spacings, such as low-frequency lattice vibrations and "beats" corresponding to the frequency difference between two Franck−Condon active vibrational modes.[62] Beating arises from the nonzero displacements of two vibrational modes whose frequency difference is much smaller than the sum of the two frequencies. Because the a_{1g} stretching mode is the highest frequency, progression-forming mode in the title systems, there must be a vibrational mode that is approximately 25−35 cm^{-1} higher in frequency to achieve the small repetitive spacing effect observed in the spectra of the thiocyanate complexes. Raman spectra measured at 300 and 77 K and those reported in literature studies[31] reveal that there are no modes that match this description. If such a mode existed, its inclusion in our model would result in a calculated spectrum with a large discrepancy in the vibronic intervals on the red side of the spectra, i.e., an increase of the a_{1g} interval as opposed to the observed decrease for the platinum(II) thiocyanates **1** and **2**. The 5 K luminescence of **1** (Figure 2a) exhibits the same small frequency interval of ca. 35 cm^{-1} as observed in the spectra of **2** and **3** (Figures 3a and 4a), in addition to other intervals of 70 and 10 cm^{-1}. In the 10 K luminescence spectrum of complex **3** the small repetitive spacings of 35 cm^{-1} are the most resolved and persist close to the band maximum. Because small spacings in the same approximate interval are present in different complexes and in the same complexes in different crystalline environments, lattice vibrations with large displacements are probably not responsible for these features. We rationalize the small repetitive spacings based on the previous considerations of odd-parity vibrational modes, i.e., a_{2u} and the lower frequency e_u, producing two vibronic origins separated by a small frequency interval ($\Delta\hbar\omega \approx 25-35$ cm^{-1}). It has also been demonstrated on theoretical grounds that such unusual spectroscopic features can be present in the electronic spectra of square-planar complexes with second- or third-row transition metal centers, i.e., large spin−orbit coupling constants.[63]

Calculated Emitting-State Distortions from Progressions in Luminescence Spectra. We use a model for the luminescence spectra of the title complexes with multiple displaced vibrational modes based on two vibronic origins. The interval between these origins is ca. 35 cm^{-1}, corresponding to the difference between the a_{2u} and the lower frequency e_u promoting vibrations. Two spectra are calculated with significant displacements in totally and non-totally symmetric even-parity metal−ligand vibrational modes and added for the resulting fitted spectrum. The time-dependent theory of luminescence spectroscopy is used to calculate the vibronic patterns in the low-temperature luminescence spectra of the title complexes and determine the magnitudes of excited-state displacements along multiple vibrational modes.[43−45] Here we only briefly discuss our application and the choice of model that we use to calculate our spectra.

Upon emission of a photon from a molecule in the emitting state at $t = 0$, a wave packet is created on the final potential energy surface. Because the wave packet is not an eigenfunction of this surface, it evolves in time according to the time-dependent Schrödinger equation. In many transition metal compounds, there are nonzero displacements of the initial and final state potential surfaces along multiple vibrational modes. The wave packet will then follow the path of steepest descent, which governs the overall width of the luminescence band. The intensity of the luminescence transition is given by eq 1,

$$I_{\mathrm{lum}}(\omega) = C\omega^3 \int_{-\infty}^{+\infty} e^{i\omega t}\langle\phi|\phi(t)\rangle\, dt \qquad (1)$$

where $I_{\mathrm{lum}}(\omega)$ is the luminescence intensity at the frequency ω, C is a constant, and $\langle\phi|\phi(t)\rangle$ is the autocorrelation function, which is the overlap of the initial wave packet, $\phi(t = 0)$, with the time-dependent wave packet, $\phi(t)$.

The latter quantity is calculated from a closed-form analytical equation,[43−45] and several assumptions have to be made in order to calculate the overlap in a multidimensional case: (a) there are no changes in the vibrational force constants in the excited state; (b) there is no mixing of normal coordinates; and (c) the transition dipole moment, μ, is constant. The overlap for the kth mode is then given by eq 2,

$$\langle\phi_k|\phi_k(t)\rangle = \exp\left[-\frac{\Delta_k^{\,2}}{2}(1 - \exp(-i\omega_k t)) - \frac{i\omega_k t}{2}\right] \qquad (2)$$

for harmonic potential energy surfaces Δ_k *and* ω_k are the displacement and frequency of the kth mode in dimensionless units and cm^{-1}, respectively. For many displaced modes, the total overlap is the product of overlaps for each individual mode,

$$\langle\phi|\phi(t)\rangle = \prod_k \langle\phi_k|\phi_k(t)\rangle \exp\left(\frac{-iE_0 t}{\hbar} - \Gamma^2 t^2\right) \qquad (3)$$

where E_0 is the energy of the electronic origin and Γ is a Gaussian damping factor, both in cm^{-1}. After calculating the total overlap, the result is Fourier transformed (eq 1) to give the spectrum.

(62) Hollingsworth, G. J.; Shin, K.-S. K.; Zink, J. I. *Inorg. Chem.* **1990**, *29*, 2501.
(63) Ballhausen, C. J. *Theor. Chim. Acta* **1965**, *3*, 368.

Table 3. Parameters Used To Calculate Luminescence Spectra of the Title Complexes

parameter	$[Pt(SCN)_4](PPh_4)_2$ (**1**)	$[Pt(SCN)_4](n\text{-}Bu_4N)_2$ (**2**)	$[Pd(SCN)_4](n\text{-}Bu_4N)_2$ (**3**)	$[Pt(SeCN)_4](n\text{-}Bu_4N)_2$ (**4**)	$[Pd(SeCN)_4](n\text{-}Bu_4N)_2$ (**5**)
progression	**I**, **II**[d]	**I**, **II**[d]	**I**, **II**[d]	**I**	**I**
vibrational energies [ground and emitting states] (cm^{-1}): normal coordinate offset (dimensionless)	295[a,b]: 4.01, 3.87 285[b,c]: 1.00, 1.00 250[a]: 1.64, 1.52 175[b]: 0.71, 0 145[a,b]: 1.18, 1.00 110[a]: 1.05, 0.71	303[a,b]: 3.75, 3.67 290[a,b]: 0.71, 0.55 257[b]: 1.92, 1.55 151[a,b]: 1.22, 1.22 132[b]: 1.05, 0.84	274[a,b]: 3.55, 3.53 260[b,c]: 1.48, 1.45 140[a,b]: 1.67, 1.64 113[b]: 1.14, 0.84	195[a,b]: 4.36 160[a,b]: 1.73 105[a,b]: 1.87 65[c]: 1.0	185[a,b]: 4.22 145[a,b]: 1.79 110[a,b]: 1.84 65[c]: 0.89
E_0 (cm^{-1})	**I** 17464 **II** 17387	**I** 16806 **II** 16771	**I** 14343 **II** 14307	**I** 16330	**I** 14445
Γ (cm^{-1})	10	10	6	15	15
% $\Delta_{a_{1g}}/\Delta_{total}$	42 (I), 48 (II)	43 (I), 47 (II)	45 (I), 47 (II)	49 (I)	48 (I)

[a] From luminescence. [b] Experimental Raman frequency measured at 295 K. [c] Raman and IR.[31] [d] Progression II is scaled by an appropriate factor and added to progression I; (**1**) 0.15, (**2**) 0.35, (**3**) 0.70.

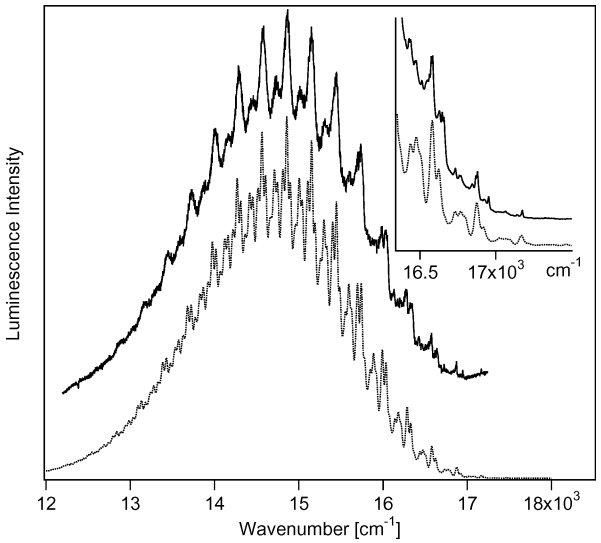

Figure 9. Calculated and experimental (5 K) luminescence spectra of **1**. The experimental spectrum is offset along the ordinate, and the calculated spectrum is given by the dotted trace. The inset shows features near the origin. All parameters used for the calculated spectrum are listed in Table 3.

The primary goal of calculating the luminescence spectra is to determine excited-state distortions, Δ_k, along the displaced vibrational modes and to rationalize the apparent anharmonicity effects. Table 3 shows the numerical values used in the calculation of luminescence spectra of the title complexes. In complexes **1**−**3**, we calculate luminescence spectra using two origins separated by the frequency difference of two promoting modes whose frequency difference corresponds to the small repetitive spacing observed in the luminescence spectra of these complexes (ca. 35 cm^{-1}). The calculated spectra shown in Figures 9−12 are obtained by first fitting one progression (progression **I** in Table 3) followed by calculating the second progression (progression **II**) and scaling it by appropriate factors, which are 0.15 (**1**), 0.35 (**2**), and 0.70 (**3**). Values used for the individual offsets, Δ_k, of both progressions are varied independently to obtain reasonable fits for the experimental spectra. The final result is obtained by adding the two calculated spectra. In cases where the luminescence is vibronically allowed, the propagating wave packet is multiplied by the transition dipole and along each displaced mode the cross sections explored are not necessarily identical. The procedure used to calculate spectra is justified by the need to reproduce the highly

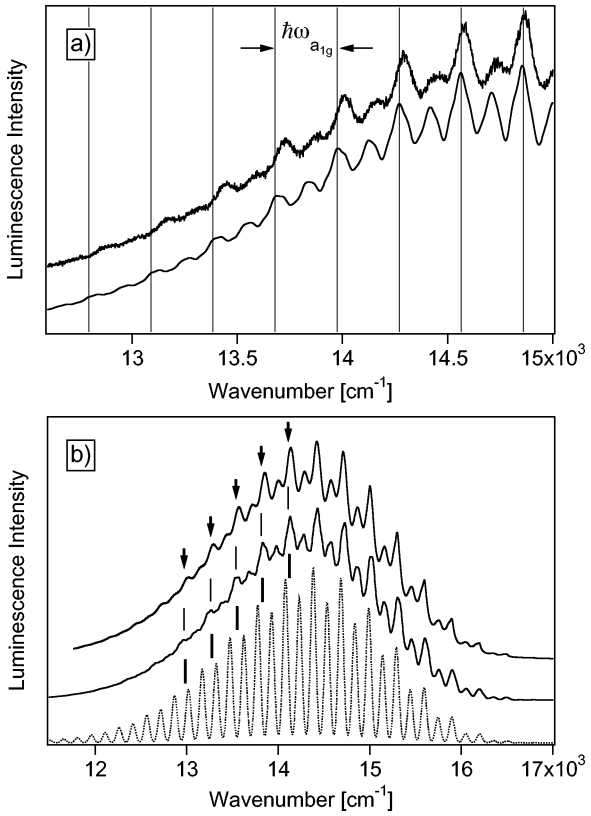

Figure 10. (a) Calculated (Γ = 15 cm^{-1}) and experimental (5 K) luminescence spectra of **1** on the lower energy half of the spectrum. The experimental spectrum is offset, and the vertical lines represent intervals of the totally symmetric Pt−S stretching mode (a_{1g}, 295 cm^{-1}). (b) Calculated and experimental luminescence spectra of **2**. The top trace is the experimental spectrum at 5 K, the middle trace represents the 5-mode calculated spectrum with two vibronic origins (Γ = 10 cm^{-1}) using the parameters in Table 3, and the bottom trace is a 2-mode model (Γ = 20 cm^{-1}) calculated spectrum. To illustrate the decrease of the high-frequency progression interval on the low-energy side of the spectrum, the intervals of the highest frequency are indicated on the experimental spectrum by arrows. Corresponding lines are given on the calculated spectra for comparison to the experimental trace.

resolved features in Figures 1−4, and we obtain the differences between progressions on different vibronic origins by using individual offsets for both the calculated spectra. This does not lead to substantial differences in offsets between the largest displaced modes. Spectra calculated using exactly identical offsets for progressions built on both vibronic origins **I** and **II** resulted in noticeable discrepancies between the best-fit spectrum and the experimental data, as

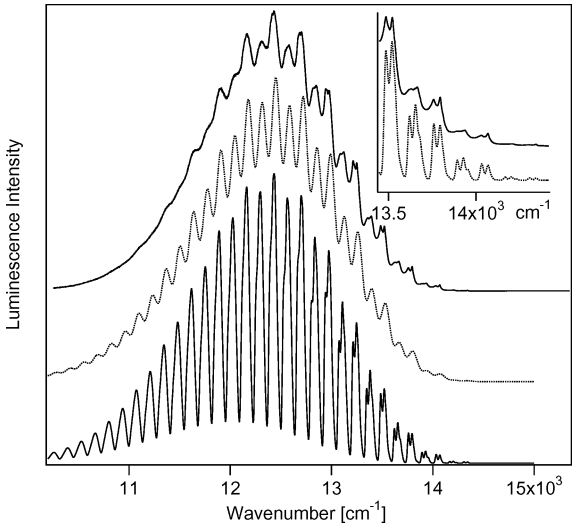

Figure 11. Calculated and experimental spectra of $[Pd(SCN)_4](n\text{-}Bu_4N)_2$ **3**. The top trace denotes the 10 K experimental spectrum, the dotted (middle) trace is a 4-mode calculated spectrum ($\Gamma = 32$ cm^{-1}) with one origin, and the solid (bottom) trace is the best-fit high-resolution 4-mode calculated spectrum with two vibronic origins ($\Gamma = 4$ cm^{-1}). Both calculated spectra use the same vibrational modes. The offsets (Δ) for the single-origin calculated spectrum are as follows: $\Delta_{274} = 3.36$, $\Delta_{260} = 1.76$, $\Delta_{140} = 1.52$, and $\Delta_{113} = 1.00$ (E_0 =14343 cm^{-1}). Parameters for the 2-origin fit are listed in Table 3. The inset shows the experimental spectrum (solid trace) and 2-origin calculated spectrum (dotted trace) highlighting the small doubling effect.

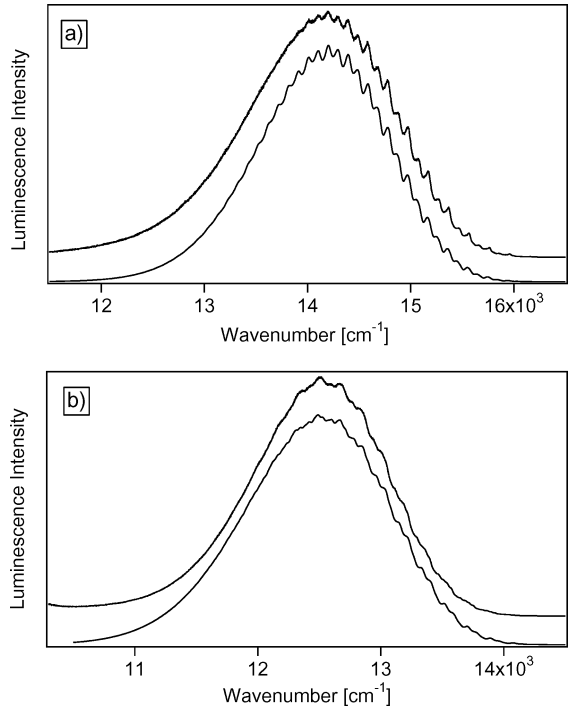

Figure 12. (a) Calculated spectrum (bottom trace) and experimental spectrum (top trace) of $[Pt(SeCN)_4](n\text{-}Bu_4N)_2$ **4** at 6 K. (b) Calculated spectrum (bottom trace) and experimental spectrum (top trace) of $[Pd(SeCN)_4](n\text{-}Bu_4N)_2$ **5** at 6 K. Parameters used in the calculated spectrum are listed in Table 3.

shown in the Supporting Information. Low-temperature luminescence spectra of complexes **4** and **5** have a much narrower spectral profile, and vibronic structure is not as resolved near the origin. We use only one origin to calculate the luminescence spectra for these compounds, which leads to very good agreement with the experimental spectra as shown in Figure 12. All vibrational frequencies used in the calculations are determined from experimental Raman spectra. The percentage of the a_{1g} displacement to the sum of all normal coordinate offsets is listed at the bottom row of Table 3. The variance of this value between complexes with the same ligand is small, which shows that all complexes, despite the differences in bandwidths, have similar displacements along the dominant progression-forming mode. The values used for the damping factor, Γ, in the calculated luminescence spectra for complexes **1**−**3** are smaller than the actual vibronic bandwidths. This was necessary due to the "filling in" effects by the large number of displaced modes of closely spaced progressions and to show the small doubling effect near the origin region. The choice of Γ does not influence the values of Δ_k used to calculate the spectra in Figures 9−12.

Figure 9 shows the fit for complex **1**. A larger frequency interval, 70 cm^{-1}, is used between the two vibronic origins **I** and **II** corresponding to the largest separation between dominant progressions observed in the experimental spectrum in Figures 1 and 2a. The inset in Figure 9 is the origin region showing the good agreement between the calculated and experimental spectra. Some of the detailed features, such as the small spacings of 10 cm^{-1}, cannot be reproduced in the calculated spectra due to the overlapping of several peaks and the value of the damping factor, Γ. Figure 10a shows the low-energy side of **1** with the calculated spectrum ($\Gamma =$ 15 cm^{-1}) below the experimental spectrum. The vertical lines correspond to constant frequency intervals in the a_{1g} mode (295 cm^{-1}), illustrating the effect of a gradually decreasing frequency interval of the main progression in the experimental spectrum. Figure 10b shows the experimental (top trace) and calculated (bottom and middle traces) spectra of **2** with the arrows at the maxima of selected vibronic peaks on the low-energy side. When using a simpler model based on one origin with only the two predominant displaced modes (a_{1g} and b_{2g}), the calculated spectrum (bottom trace) cannot reproduce the experimental spectrum, as shown by the vertical lines that match the largest frequency interval in the experimental spectrum. The best-fit calculated spectrum with two vibronic origins can better reproduce the decrease in the largest progression interval on the red side as well as the small doubling effect near the luminescence origin. Figure 11 contains the experimental (top trace) and calculated (bottom and middle traces) luminescence spectra of **3**, and the inset shows the origin region in detail. The two-vibronic-origin model is able to reproduce the small repetitive spacing and the intensity distributions of the individual progressions. We include a best fit to the overall band profile using a single-origin spectrum with the same vibrational modes involved as a comparison. Figure 12 shows the experimental (top traces) and calculated (bottom traces) of the selenocyanate complexes **4** and **5**. It was found that a model based on one origin, considering the number of vibrational modes involved, was sufficient to calculate the luminescence spectra. Preliminary calculations with the two-origin model lead to congested spectra and poor agreement between calculated and experimental spectra. This discrepancy is attributed to

the fact that the luminescence spectra of the selenocyanates are much narrower than those of the thiocyanate analogues, making the fit procedure difficult with the two-origin model due to the many overlapping vibronic bands.

Phenomenological spectroscopic effects reminiscent of those analyzed here have been observed for other compounds. The low-temperature luminescence spectrum of bis(maleonitriledithiolato)palladate(II) shows highly resolved vibronic structure that is "modulated" by a small frequency interval of 26 cm^{-1}.[53] The origin of this small repetitive spacing arises from a beating effect, and the two modes with largest displacements have a frequency difference of 26 cm^{-1}. Another illustrative example is the low-temperature luminescence spectrum of ruthenocene, which exhibits two well-defined progressions in the totally symmetric (a_{1g}) Ru−cp stretching mode with the main vibronic peaks separated by 165 cm^{-1}.[62] Similar beating effects occur in this spectrum with well-resolved shoulders appearing on the two main progressions. The beat frequency comes from differences between the totally symmetric stretching mode and higher frequency non-totally symmetric modes. In both the above cases, we find that similar models applied to the spectra in Figures 1−4 do not yield good fits or are physically meaningless. Overall, the calculated fits are able to reproduce the important and prominent spectral features observed in the experimental luminescence spectra, and we now use the time-dependent theory to explain the effect of the decreasing main progression interval across the luminescence bands.

Non-Constant Progression Intervals. From the high-resolution luminescence spectra of **1**−**3**, we have found that there are significant displacements in non-totally symmetric vibrational modes, including the b_{1g} and b_{2g} stretching and bending modes. Near the luminescence band maxima, the resolution decreases and only the dominant progressions are visible. In this region, transitions near the maxima of the a_{1g} progression coalesce and appear as one peak. In the model defined by eqs 1−3, this effect corresponds to a damping factor, Γ, that increases as the luminescence energy decreases. Multiple individual maxima for the narrow vibronic peaks are resolved near the origin, but only a single maximum is observed for the broader vibronic peaks at lower energy that does not exactly correspond to any ground-state vibrational frequency, as indicated by the arrows in Figure 10b. This effect causes a gradual decrease of the experimental energy interval separating maxima of the main apparent progression in the spectra of the thiocyanate complexes, giving the overall impression of anharmonicity. A well-established and related effect has been reported for $K_2[PtCl_4]$, where large displacements along the a_{1g} mode and smaller displacements along the lower frequency b_{1g} mode give an overall progression frequency that does not match the frequency of any ground-state vibrational mode.[39] This is known as the "missing mode effect", or MIME, and is observed when vibronic progressions are not highly resolved. The decrease of the progression interval on the low-energy side of the luminescence spectra of **1** and **2** (Figures 1, 2, 3a, and 4a) is different from the MIME effect, but can be rationalized with the concepts underlying the MIME. From the calculations using the harmonic approximation with multiply displaced vibrational modes we are able to show that the decrease in the main progression interval comes from changes in the relative intensities of individual vibronic transitions and *not* from an anharmonic shape of the potential energy surface.

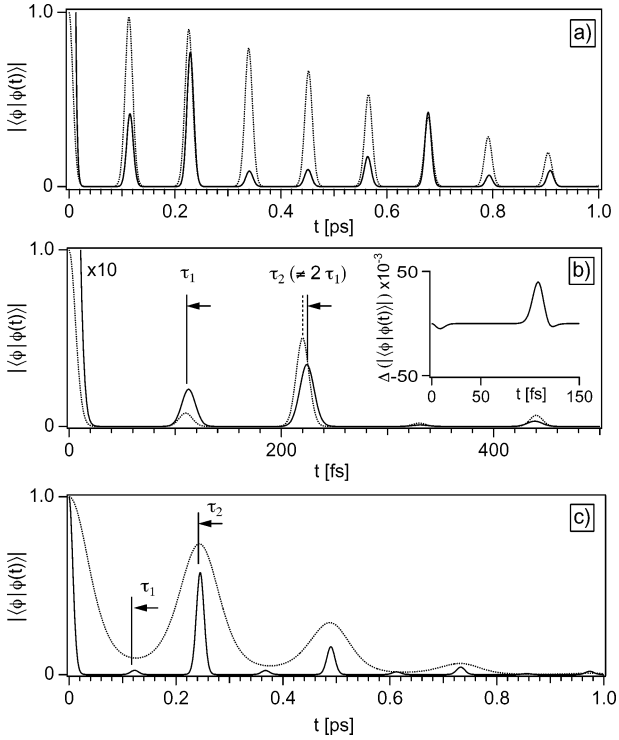

Figure 13. (a) Absolute autocorrelation functions for **1**. Dotted trace: autocorrelation function for the 295 cm^{-1} mode ($\Gamma = 10$ cm^{-1}). Solid trace: total autocorrelation used to calculate the best-fit spectrum and enlarged by a factor of 10. (b) Total autocorrelation functions for calculated spectra of **2**. Solid trace: total autocorrelation of the two-vibronic-origin best-fit spectrum enlarged by a factor of 5. Dashed trace: 2-mode total autocorrelation. The first two recurrence times are indicated (τ_1, τ_2) showing that $\tau_2 \neq 2\tau_1$. Inset: difference plot showing the mismatch in the second recurrence times for the total autocorrelation of the best-fit spectrum. (c) Total autocorrelation functions for calculated spectra of **3**. Solid trace: total autocorrelation used in the high-resolution two-vibronic-origin model calculated spectrum ($\Gamma = 6$ cm^{-1}). The dotted line is included as a guide for the eye to show the modulation of the overlap.

The time-dependent theory allows for an intuitive understanding of these features. Figure 13 shows calculated absolute autocorrelation functions for the spectra in Figures 9−12. The top panel (Figure 13a) shows the total overlap used for the calculated spectrum of **1** (Figure 9) with the overlap of the single a_{1g} mode (295 cm^{-1}) using the average displacement value from the calculated spectrum. The second recurrence of the overlap shows a small mismatch with the expected recurrence time of the 295 cm^{-1} mode. The middle panel (Figure 13b) shows the absolute overlaps used in the calculated spectra of Figure 10b. The inset of Figure 13b is the difference in absolute autocorrelation functions ($\Delta|\langle\phi|\phi(t)\rangle|$) between a two-mode model and the model for the best-fit calculated spectrum. The recurrence mismatch can be clearly seen in the second recurrence, where the best-fit spectrum has a longer recurrence time compared to what would be expected for progressions with constant energy spacings between members. This mismatch is the result of two vibrational modes close in frequency, i.e., a_{1g} and b_{1g}

modes, that combine to yield a frequency that does not correspond to any ground-state vibration, as is illustrated in Figure 10a. The actual MIME frequency is then mediated within the range of each implicated mode by the individual offsets for these modes. The bottom panel (Figure 13c) contains the absolute autocorrelation used to calculate the spectrum of **3** (Figure 11). The overlap is modulated by beats that are illustrated by the dotted trace. The beat frequency arises out of the difference between the two highest frequency modes with the largest displacements. It corresponds to 136 cm^{-1}, which is the difference of the a_{1g} and b_{2g} frequencies. The b_{1g} mode also has a significant distortion, but its beat with the a_{1g} modes is only 14 cm^{-1} and may only manifest itself at longer time scales than necessary for our calculations. Similar beat effects occur for the selenocyanate complexes where the a_{1g} and b_{2g} modes also have the largest displacements.

Temperature- and Pressure-Dependent Luminescence Decay Behavior. Large displacements of the emitting-state potential energy surface along multiple normal coordinates favor nonradiative decay mechanisms because the potential surfaces of the ground and excited states cross at energies close to the lowest vibrational level of the emitting state. At room temperature (ca. 300 K) efficient nonradiative relaxation processes lead to short luminescence lifetimes and weak luminescence intensities. This situation corresponds to the strong-coupling limit[46] of radiationless decay theory where the transition probability for nonradiative decay depends exponentially on the activation energy between the two states in the luminescence transition. One of the classical spectroscopic characteristics for the strong-coupling case is when the Stokes shifts are much larger than the largest accepting vibrational frequency, as observed for the title complexes in Figures 1−4 and summarized in Table 1. We use an analytical expression for the nonradiative rate constant, k_{NR}, derived by Englman and Jortner[46] to model the temperature-dependent luminescence decay behavior.

$$k_{NR} = \frac{C_{ij}^{\,2}\sqrt{2\pi}}{\hbar\sqrt{E_m k_B T^*}}\, e^{(-E_A/k_B T^*)} \qquad (4)$$

C_{ij} is a pre-exponential frequency factor, k_B is the Boltzmann constant in cm^{-1}/K, $\hbar$ is in units of $cm^{-1}\cdot s$,

$$k_B T^* = \frac{1}{2}\hbar\omega_{eff}\coth\left(\frac{\hbar\omega_{eff}}{2k_B T}\right) \qquad (5)$$

and

$$E_A = \frac{(\Delta E - E_m)^2}{4E_m} \qquad (6)$$

where ΔE is the energy difference between the lowest vibrational levels of the ground and emitting states, (E_0) in Table 1, and E_m is half the Stokes shift,

$$E_m = \frac{1}{2}\sum_i^N \hbar\omega_{eff}\Delta_k^{\,2} \cong \frac{1}{2}\hbar\omega_{eff}\Delta_{total}^{\,2} \qquad (7)$$

Table 4. Parameters Used in the Calculation of the Nonradiative Rate Constant within the Strong-Coupling Model in Eq 4

parameter	$[Pt(SCN)_4]$-$(n\text{-}Bu_4N)_2$ (**2**)	$[Pd(SCN)_4]$-$(n\text{-}Bu_4N)_2$ (**3**)	$[Pt(SeCN)_4]$-$(n\text{-}Bu_4N)_2$ (**4**)	$[Pd(SeCN)_4]$-$(n\text{-}Bu_4N)_2$ (**5**)
ΔE (cm^{-1})[a]	16806	14343	16330	14445
C_{ij} (cm^{-1})	18	85	2700	1400
Δ_{total}	8.25	7.66	8.96	8.74
$\hbar\omega_{eff}$ (cm^{-1})[b]	251	220	155	146

[a] Line 2 (E_0) in Table 1. [b] The contribution to $\hbar\omega_{eff}$ from each displaced mode is weighted by the individual offsets in Table 2.

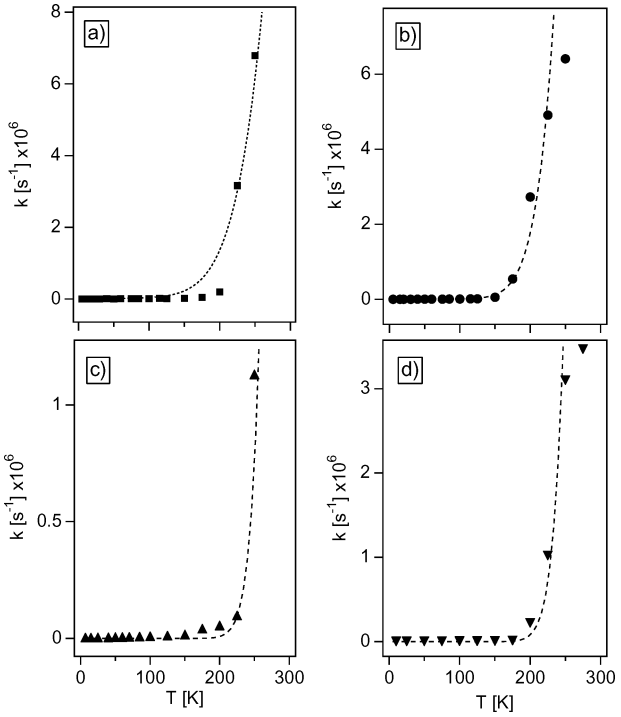

Figure 14. Experimental luminescence decay rate constants (solid symbols) with calculated fits using eq 4 (dashed lines) as a function of temperature: (a) $[Pt(SCN)_4](n\text{-}Bu_4N)_2$ **2**; (b) $[Pt(SeCN)_4](n\text{-}Bu_4N)_2$ **4**; (c) $[Pd(SCN)_4](n\text{-}Bu_4N)_2$ **3**; (d) $[Pd(SeCN)_4](n\text{-}Bu_4N)_2$ **5**.

The effective accepting mode, $\hbar\omega_{eff}$, is calculated as the weighted sum of all displaced metal−ligand vibrational frequencies (in cm^{-1}), listed in Table 3. Δ_{total} is the offset between the ground- and excited-state potential minima (dimensionless units), which is taken as the sum of all Δ_k used to calculate the spectra (Table 3). For the thiocyanate complexes (**2** and **3**) we use the average Δ_k values for progressions **I** and **II** then sum over these averaged offsets for Δ_{total}. Identical frequencies for the accepting mode in the ground and emitting states are assumed in the Englman−Jortner formalism provided that the energy difference between these states is sufficiently large. The only nonempirical parameter in eq 4, C_{ij}, is assumed to be a constant and adjusted to obtain good fits with experimental decay rate data as a function of temperature. The observed luminescence decay rate constants are then modeled with eq 4 assuming that the radiative rate constant, k_R, is equal to the observed rate at 5 K ($k_{NR} = 0$) and is invariant of temperature. The parameters used in the calculations are collected in Table 4. Figure 14 shows good agreement between the one-parameter fits with the observed temperature-dependent decay rate constants for complexes **2**−**5**. Some discrepancies arise

between 150 and 200 K for complexes **2** and **4**, where the calculated rate constant increases faster than the experimental data for the former, and slower for the latter. However, experimental rates for both complexes show a rather sudden increase at 225 K, and this large change may contribute to the difficulty of reproducing these trends in the data at higher temperatures. Because the title complexes undergo multiple and substantial distortions in the excited states, this simple one-dimensional model cannot fully account for all possible contributions to the observed luminescence decay rate constants. This is most obvious in the large differences between individual values used for C_{ij}, and, due to the inherent difficulty of accurately estimating such coupling factors, we do not attempt to interpret these quantities. The most important aspect of this model is that reliable calculated decay rate constants can be obtained by using parameters determined directly from resolved experimental spectra and quantitative calculated luminescence spectra. The Englman−Jortner expression (eq 4) is now used to rationalize the pressure-dependent luminescence decay behavior of complexes **2**−**5** in Figures 6−8.

Pressure-Dependent Luminescence Intensities and Lifetimes. At room temperature and ambient pressure the luminescence spectra of the title complexes are very weak. The large pressure-induced enhancements of the luminescence intensities observed for the title complexes are unexpected, and they can principally arise from both increasing radiative relaxation rate constants and decreasing nonradiative relaxation rate constants. The trends observed here are comparable to some organic chromophores that show enhancements of luminescence intensities and lifetimes with increasing pressure.[16] A possible contribution to the increase in intensity as a function of pressure may be caused by the removal of the center of inversion, thereby making the electronic transition more allowed in a non-centrosymmetric molecular geometry. The nature of the metal−ligand geometry and specific vibrational modes may also play an important role in this process. For example, by compressing the crystals the bending motions (b_{2g}) can gain "leverage" through intermolecular forces acting on the SCN^- and $SeCN^-$ ligands. This effect would enable the metal-centered luminescence transition to be tuned through these largely displaced, low-frequency bending vibrations in the emitting state. To test the validity of this conjecture, we have measured the pressure-dependent luminescence spectra of $K_2[PdBr_4]$, a compound that does not show a progression in the b_{2g} mode.[37] The room-temperature luminescence of this compound is weak, similarly to the title complexes, and there was virtually no pressure-induced enhancement of the signal.

The luminescence lifetimes also exhibit a considerable increase from ambient pressure values as shown in Figure 8 and Table 2. If the pressure-induced changes in molecular structure remove the center of inversion around the metal ion, the luminescence transition becomes more allowed and the lifetime is expected to decrease as the radiative rate constant, k_R, increases. In contrast, the measured decay rate constant decreases significantly. The decrease of the rate constant by more than 2 orders of magnitude indicates

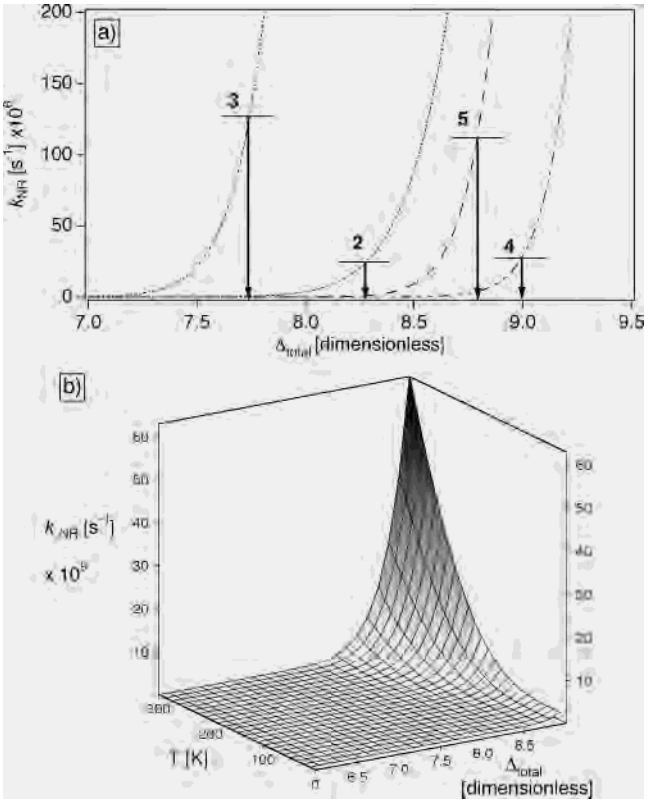

Figure 15. (a) Calculated nonradiative rate constants (k_{NR}) as a function of the normal coordinate offset (Δ_{total}) along the $\hbar\omega_{eff}$ at 300 K. The downward arrows indicate the value of Δ_{total} used for the calculation of temperature-dependent rate constants in Table 4. (b) k_{NR} calculated as a function of temperature, T, and emitting-state offset, Δ_{total}, along the effective mode, $\hbar\omega_{eff}$, of complex **3**.

therefore a very large decrease of the nonradiative rate constant, k_{NR}, with pressure. To better understand the trend in pressure-dependent lifetimes, we apply the strong-coupling model discussed in the previous section to the pressure-dependent decay rates.

The model described by eq 4 treats the title complexes as isolated molecules. At pressures greater than 30 kbar it is obvious that intermolecular effects are increasingly important since the spectra show steady decreases in intensity due to quenching by efficient energy transfer to nonluminescent traps. This situation is not addressed by eq 4, and we instead focus on the rise in luminescence intensities and lifetimes with pressure below 30 kbar. The most relevant pressure-dependent parameter in the strong-coupling model is the offset along the effective accepting mode, Δ_{total}. Figure 15a shows the effects of varying Δ_{total} on k_{NR} at a constant temperature of 300 K for complexes **2**−**5** to simulate the effect of pressure-induced decreases in normal coordinate offsets between the ground and emitting states. Figure 15b shows the surface generated by varying both temperature, T, and Δ_{total} for complex **3**.

From Figure 15a, it is clear that the variation of k_{NR} with Δ_{total} near the values of Δ_{total} used in the calculation of temperature-dependent decay rate constants (indicated by the downward vertical arrows) is greater for the palladium(II) complexes **3** and **5** than for the platinum(II) complexes **2** and **4**, resulting in a larger decrease in k_{NR} for similar

decreases in Δ_{total}. This result is consistent with the trends of the experimental pressure-dependent luminescence decay rate constants and intensities in Figures 6−8. The variations of k_{NR} calculated with eq 4 are similar for complexes of the same metal ion, despite the very different C_{ij} values used for different ligands. The most important differences between the platinum(II) and palladium(II) complexes that influence the dependence of k_{NR} as a function of Δ_{total} are the vibrational frequencies, the offsets Δ_{total}, and the luminescence energies (ΔE in eq 6). Each of these parameters alone is not sufficient to explain the pressure-induced luminescence effect. For example, a large value of Δ_{total} leads to a lower activation barrier for nonradiative relaxation than a small value of Δ_{total}, suggesting a large rate constant for identical $\hbar\omega_{eff}$ and luminescence energy. Figure 15a shows that the platinum(II) complexes have larger Δ_{total} values than their palladium(II) analogues, but their k_{NR} values are lower and vary less than those of the palladium(II) complexes. The observed variations are determined by all these parameters simultaneously. The lower vibrational frequencies of the palladium(II) complexes lead to wider potential energy surfaces and crossings at lower activation energy for identical Δ_{total} and luminescence energy, and their lower luminescence energies also lead to lower activation energy barriers, assuming identical Δ_{total} and $\hbar\omega_{eff}$ values. The influence of all these parameters determines the slope of the surface shown for one compound (**3**) in Figure 15b and for three others (**2**, **4**, and **5**) in the Supporting Information. An alternative, qualitatively appealing rationalization of the pressure effect on luminescence properties is given by the variation of the activation energy, defined in eq 6 as the difference between the minimum of the emitting-state potential energy curve and the crossing point of the ground- and emitting-state potential curves given by the parameters in Table 4. For identical variations of Δ_{total}, a larger change of the activation energy is obtained for the palladium(II) complexes than for the platinum(II) complexes, confirming the trends summarized in Figures 6−8. The variations of the activation energies (eqs 6 and 7) for compounds **2**−**5** as a function of Δ_{total} are given in Figure S12 of the Supporting Information. This comparison illustrates that the analysis of the pressure effects reported here does not depend on the mathematical formalism chosen to describe the nonradiative rate constants, but that their physical origin can be understood from the emitting-state potential energy surfaces derived from the low-temperature luminescence spectra.

Transitions between states with small Δ_k along metal−ligand vibrational modes, such as intraconfigurational d−d and some charge transfer transitions, are expected to show small changes in the pressure-dependent luminescence lifetimes at a constant temperature. For example, the pressure-dependent excited-state decay kinetics for $[Ru(bpy)_3]Cl_2$ and $[Ru(phen)_3]Cl_2$, both metal-to-ligand charge transfer (MLCT) emitters, were successfully modeled using an expression in the weak-coupling limit of radiationless decay theory (energy gap law) and do not show large changes of k_{NR} with pressure. The increases in pressure-dependent lifetimes of these systems are less than a factor of 2,[18,19] much smaller than those reported here. It is also expected that the role of the b_{2g} bending mode in the pressure-induced enhancements of luminescence intensities and lifetimes is important given the large displacements that occur along this mode in the emitting state. Figure 15b also shows that at lower temperatures the values of k_{NR} decrease significantly and vary much less with Δ_{total} than at room temperature. We therefore expect smaller changes of luminescence intensity at low temperatures, which might explain why $K_2[Pt(SCN)_4]$ does not appear to show an enhancement of luminescence intensity with increasing pressure at 100 K.[60] By using eq 4 and varying Δ_{total} to simulate the effect of pressure, it is also possible to explain the pressure-induced blue shifts of all luminescence band maxima. A significant decrease in Δ_{total} can lead to a significant blue shift of the band maxima without any change in the energy of the potential minimum since the more nested emitting-state surface would shift vibronic intensities toward higher energy. We suspect that energy differences between potential energy minima (electronic origins) do not change with pressure because they are similar for thiocyanate and selenocyanate complexes of the same metal ion, a much larger "spectrochemical change" than the shifts induced by the pressures used here.

Conclusions

The temperature- and pressure-dependent spectroscopic results show large variations from ambient conditions. Analysis of the vibronic structure in the low-temperature luminescence spectra shows that the largest displacements occur along the totally symmetric (a_{1g}) metal−ligand stretching vibration. Significant distortions in the b_{2g} bending modes occur in all complexes, and the pressure effects on luminescence properties are most likely dependent on the pressure-induced displacement of this mode. The strong-coupling model can be used to rationalize the temperature and pressure dependence of the nonradiative decay rate constant using physically meaningful parameters determined from spectroscopic experiments.

Acknowledgment. We thank the Natural Sciences and Engineering Research Council (Canada) for research grants and for a scholarship to J.K.G.

Supporting Information Available: Raman spectra of complexes **2**−**5**, and pressure-dependent Raman spectra of **2**. Pressure-dependent Raman spectra for **2** in the metal−ligand vibration region. Polarized luminescence spectra of complex **1**. Pressure-dependent luminescence spectra of **1**. High-resolution luminescence spectrum of **3** at 10 K showing progressions in the b_{1g} non-totally symmetric stretching mode. Luminescence lifetimes measured at 640, 670, and 700 nm for **2** fitted with single- and double-exponential functions. Angular overlap model calculations. Calculated spectra showing different choices of models for complex **1**. Autocorrelation overlaps for **4** and **5**. Activation energies (eqs 6 and 7) calculated as a function of Δ_{total} for complexes **2**−**5**. Surface plots of k_{NR} as a function of temperature and Δ_{total} for complexes **2**, **4**, and **5**. This material is available free of charge via the Internet at http://pubs.acs.org.

IC0342503